Article

Neuron

Mechanism of High-Frequency Signaling at a Depressing Ribbon Synapse

Highlights

- Vesicle docking sites at cone ribbons are slowly refilled following release
- Slow vesicle refilling is expected to limit high temporal frequency signaling
- Cones make high gain, readily saturating synapses with cb2 "Off" bipolar cells
- High gain and saturation hasten synapse recovery to enable high-frequency signaling

Authors

Chad P. Grabner, Charles P. Ratliff, Adam C. Light, Steven H. DeVries

Correspondence

s-devries@northwestern.edu

In Brief

At ribbon synapses, the rate of vesicle turnover at membrane docking sites limits high-frequency transmission. Grabner et al. identify a postsynaptic mechanism at a cone-to-"Off" bipolar cell synapse that counteracts slow turnover to enhance high-frequency signaling.

Grabner et al., 2016, Neuron *91*, 133–145
July 6, 2016
http://dx.doi.org/10.1016/j.neuron.2016.05.019

CellPress

Neuron
Article

Mechanism of High-Frequency Signaling at a Depressing Ribbon Synapse

Chad P. Grabner,[1,2] Charles P. Ratliff,[1,3] Adam C. Light,[1,4] and Steven H. DeVries[1,*]
[1]Departments of Ophthalmology and Physiology, Feinberg School of Medicine, Northwestern University, Chicago, IL 60611, USA
[2]Present address: Max Planck Institute for Biophysical Chemistry, Am Fassberg 11, 37077 Göttingen, Germany
[3]Present address: Jules Stein Eye Institute and Department of Ophthalmology, University of California, Los Angeles, Los Angeles, CA 90095, USA
[4]Present address: WaveMetrics, Inc., Lake Oswego, OR 97035, USA
*Correspondence: s-devries@northwestern.edu
http://dx.doi.org/10.1016/j.neuron.2016.05.019

SUMMARY

Ribbon synapses mediate continuous release in neurons that have graded voltage responses. While mammalian retinas can signal visual flicker at 80–100 Hz, the time constant, τ, for the refilling of a depleted vesicle release pool at cone photoreceptor ribbons is 0.7–1.1 s. Due to this prolonged depression, the mechanism for encoding high temporal frequencies is unclear. To determine the mechanism of high-frequency signaling, we focused on an "Off" cone bipolar cell type in the ground squirrel, the cb2, whose transient postsynaptic responses recovered following presynaptic depletion with a τ of ~0.1 s, or 7- to 10-fold faster than the τ for presynaptic pool refilling. The difference in recovery time course is caused by AMPA receptor saturation, where partial refilling of the presynaptic pool is sufficient for a full postsynaptic response. By limiting the dynamic range of the synapse, receptor saturation counteracts ribbon depression to produce rapid recovery and facilitate high-frequency signaling.

INTRODUCTION

The dynamic properties of synaptic ribbons convert simple voltage inputs into complex transmitter outputs. During repetitive stimuli, synaptic ribbons cycle between phasic and tonic release (DeVries, 2000; Grabner and Zenisek, 2013; Rabl et al., 2005; Singer and Diamond, 2003). Phasic release occurs when a rapid depolarization synchronously opens voltage-gated Ca^{2+} channels near membrane-docked and primed vesicles (Mennerick and Matthews, 1996). The abrupt rise in intracellular Ca^{2+} triggers a burst of vesicle fusion and glutamate release that causes a large, transient postsynaptic response (von Gersdorff et al., 1998). If the depolarization continues, phasic release tails into tonic or sustained release, which occurs at slower rates than phasic release, because new vesicles have to translocate to membrane docking sites and undergo priming before Ca^{2+} can trigger fusion (Jackman et al., 2009). Upon membrane hyperpolarization, Ca^{2+} channels close, but vesicle recruitment and priming continues and leads to a time-dependent replenishment of releasable vesicles, forming the basis for the next phasic episode (DeVries, 2000; Jackman et al., 2009; Singer and Diamond, 2003). The maximal phasic release can be 10- to 20-fold larger than tonic release during a comparable interval (DeVries and Schwartz, 1999). However, the size of the phasic component and its impact on subsequent signaling is not fixed but, instead, depends on a balance between the temporal frequencies that are signaled by a sensory neuron and the replenishment rate at its ribbons. High replenishment rates support transient signaling at high frequencies but incur a metabolic cost.

When depolarized in the dark, cone ribbons mediate glutamate release onto "Off" bipolar cells that express AMPA/kainate receptors (DeVries, 2000). Mammalian Off bipolar cells can be subdivided into five anatomical types that differ with respect to their morphology (Helmstaedter et al., 2013; Light et al., 2012; Tsukamoto and Omi, 2015) and temporal light responses. At least one type produces a transient membrane depolarization after a light step, whereas other types have more sustained responses (Baden et al., 2013; DeVries et al., 2006; Ichinose and Hellmer, 2015; Pang et al., 2012). The spatiotemporal interplay between responses in transient and sustained bipolar cell types may be critical for directional signaling (Kim et al., 2014), which first emerges in starburst amacrine cells. In addition, transient and sustained bipolar cells may provide input to transient and sustained ganglion cells (Cleland et al., 1971). Against the idea that the cone-to-Off bipolar cell synapse can be the origin of transient signaling over the temporal range of cone vision (up to 100 Hz) (Derrington and Lennie, 1984; Smith et al., 2001; Jacobs et al., 1980) is the observation that ribbon vesicle-docking sites are replenished with a time constant, τ, of 0.7–1.5 s (Innocenti and Heidelberger, 2008; Jackman et al., 2009; Rabl et al., 2006), equivalent to a corner frequency of ~0.2 Hz.

Mammalian cone terminals contain 20–40 membrane invaginations, unique ultrastructural specializations of unknown function, that are marked at their apex by a synaptic ribbon (Chun et al., 1996; Dowling and Boycott, 1966). In the cone-dominant retina of the ground squirrel, AMPA-receptor-expressing Off cb2 bipolar cell dendrites enter invaginations and terminate 0.1–0.2 μm from ribbon-active zones, while other Off bipolar cell types contact cones at more distant sites (0.4–0.8 μm) at the base of the terminal (Figure 1, inset) (DeVries et al., 2006;

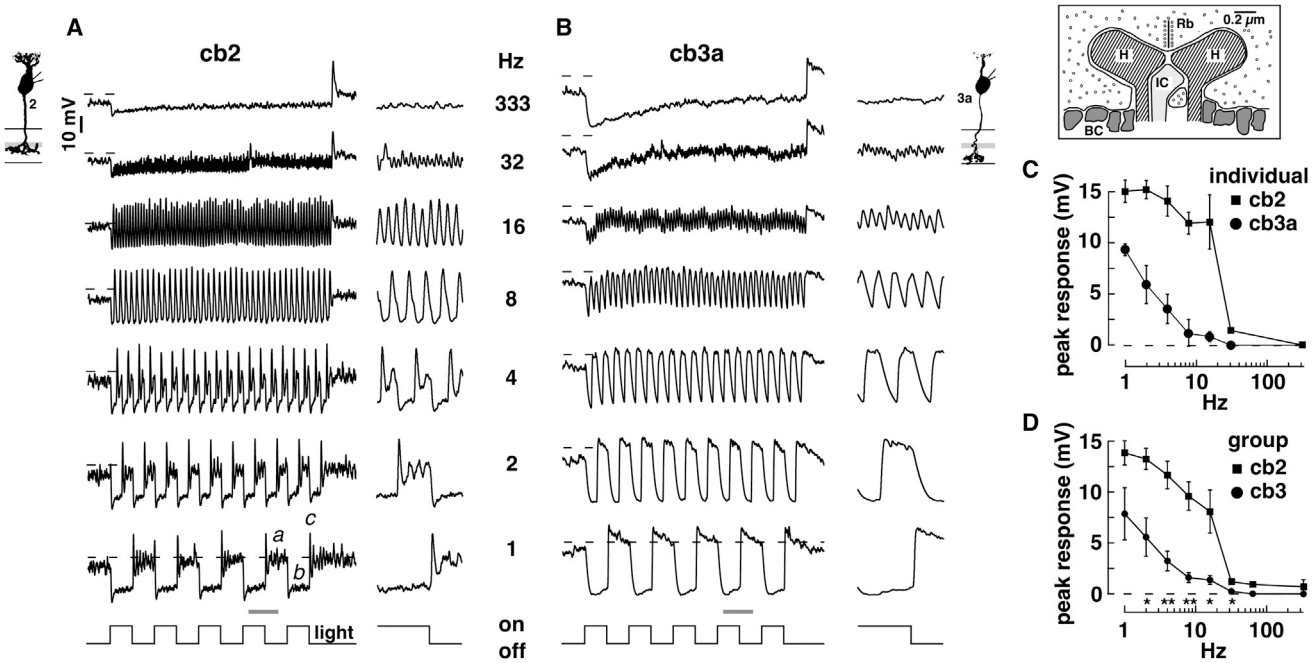

Figure 1. Depolarizing Transient Amplitude as a Function of Stimulus Frequency in cb2 and cb3 Cells

(A) Membrane voltage from a cb2 cell was recorded in current clamp during a full-field square wave light stimulus (mean = 1.7 × 10^6 photons-μm^{-2}-s^{-1}; timing is shown below for the 1-Hz trace, frequency is at the right). Baseline voltage, −50.7 mV, is defined as the average voltage during the last 100 ms of the dark phase during the 1-Hz duty cycle (dashed lines). *a*, *b*, and *c* indicate the response components before, during, and immediately after a light pulse. The gray bar shows the location of the expanded responses at right.

(B) Light responses in a cb3a cell with a baseline voltage of −40.8 mV.

(C and D) Plot of peak response amplitude relative to baseline at light-off versus frequency (C) for the cells in (A and B) (vertical bars indicate SEM, calculated from all of the light-off transitions at a frequency) and (D) for all cb2 (n = 3) and cb3 (n = 4) cells (vertical bars are SEM for the average response of each cell at a frequency). *p < 0.05 and **p < 0.005 (unpaired t test). Inset: diagram of a cone invagination showing a ribbon (Rb), and the dendritic contacts of horizontal (H), invaginating bipolar (IC), and basal bipolar (BC) cells.

Hopkins and Boycott, 1997). We hypothesize that invaginating cb2 contacts promote receptor saturation during the near-synchronous release of ribbon membrane-docked vesicles at light-off. Under saturating conditions, the replenishment and release of vesicles from a small fraction of the available docking sites can elicit a large fraction of the postsynaptic response, overcoming depression to speed up the recovery of the synaptic transient, which, in turn, facilitates high-frequency signaling. AMPA receptor saturation has been described at synapses that use action potentials, including the climbing fiber to Purkinje cell synapse (Foster et al., 2002; Harrison and Jahr, 2003; Wadiche and Jahr, 2001) and the calyx of Held (Neher and Sakaba, 2001; Sun and Wu, 2001). At these synapses, saturation promotes high-frequency signaling by providing a safety factor that combats fatigue. We show that receptor saturation also promotes high-frequency signaling during graded transmission.

RESULTS

Bipolar Cell Light Responses as a Function of Stimulus Frequency

We used temporally flickering light to screen for Off bipolar cell types that respond to high frequencies. In cb2 cells, a full-field 1-Hz square wave stimulus produced a voltage response that had three components (a, b, and c in Figure 1A). The first component was the membrane potential, V_m, in the dark (−60.1 ± 5.8 mV, n = 3; mean ± SEM), which was designated as the baseline; the second component was the hyperpolarized V_m in the light; and the third component was the transient depolarization at light-off. The peak amplitude of the transient response was 12–15 mV relative to the dark baseline level for square wave stimuli over the range of 1–16 Hz (Figure 1C; 8–14 mV for the average responses in Figure 1D). The 20%–80% rise time for the light-off transient, from hyperpolarized level to peak depolarization (30.1 ± 0.7 mV), was 7.2 ± 1.3 ms, with a width at baseline of 21.6 ± 1.5 ms (n = 5 responses during the 1-Hz stimulus). Voltage fluctuations were evident but small during a 32-Hz stimulus and were absent during a 333-Hz stimulus, presumably due to flicker fusion in cone phototransduction.

Other Off bipolar cell types lacked a transient light-off response during high-frequency flicker. Cb3a/b Off bipolar cells also had a three-component response to a square wave stimulus (Figure 1B; V_m in the dark = −45.3 ± 3.5 mV, which is not statistically different from that in cb2 cells; n = 4, p = 0.08). However, compared to cb2 cells, the responses at light-off rose more slowly (11.8 ± 1.9 ms; p = 0.002), and off-transients were reduced to <10% of their peak amplitude during flicker >4 Hz (Figures 1C and 1D). Thus, cb2 cells have a transient response

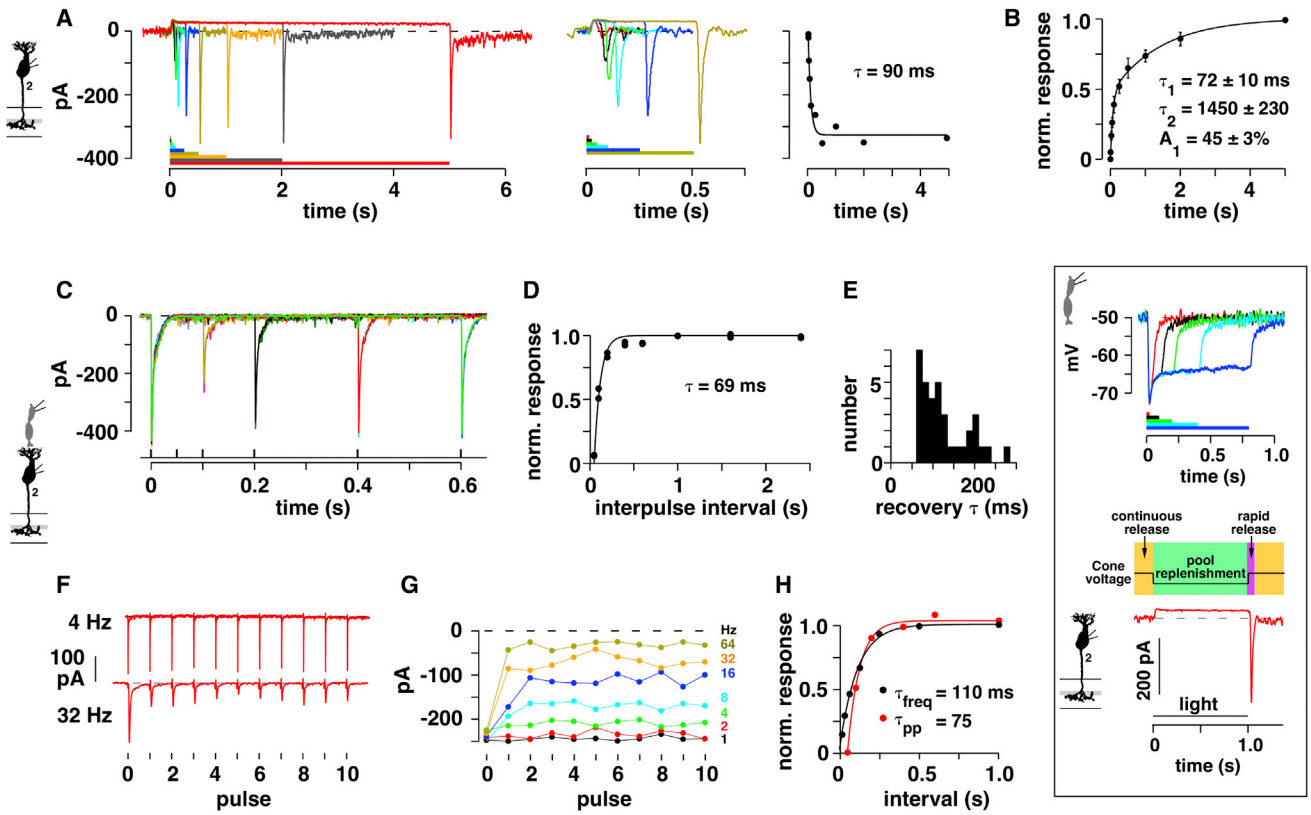

Figure 2. EPSC Recovery at the Cone-to-cb2 Cell Synapse

(A) Left: cb2 cell membrane current during a series of light pulses (4, 25, 50, 100, 250, 500, 1,000, 2,000, and 5,000 ms, shown color coded below). Stimulus intensity was 1.1×10^6 photons-μm^{-2}-s^{-1}. Middle: initial responses on a shorter timescale. Right: plot of transient peak amplitude versus light step duration fitted with an exponential curve.

(B) Plot of normalized (norm.) peak response versus step duration. The responses of individual cells were normalized to their maximum prior to averaging (n = 8). Data points were fitted by a double exponential curve. Inset, analogy between a light pulse response and the response during the two-pulse paradigm. Top: cone voltage responses during light pulses of 25, 100, 200, 400, and 800 ms, shown color coded below. Responses were uniformly hyperpolarizing. Light intensity = 3.2×10^6 photons-μm^{-2}-s^{-1}. Inset bottom: the highly primed vesicle pool is depleted when cones are depolarized in the dark, producing an inward current in a bipolar cell. Replenishment occurs when cones are hyperpolarized during the light step, which corresponds to the interpulse interval. At light-off, cones return to the dark, depolarized level. Ca^{2+} channels open and produce a near-synchronous vesicle fusion.

(C) Superimposed cb2 cell responses obtained at different interpulse intervals (two repeats at each interval). A presynaptic cone was depolarized for 1 ms in the loose-seal configuration to a voltage that produced a maximal EPSC response.

(D) Plot of normalized recovery versus interpulse interval from the data shown in (C), including points from longer intervals not shown. Recovery was fitted with an exponential curve.

(E) Histogram of recovery time constants (n = 35 pairs).

(F) EPSC responses from a different cone-to-cb2 cell pair during a train of eleven 1-ms depolarizations at 4 and 32 Hz.

(G) Plot of peak response versus pulse number for all stimulus frequencies (1–64 Hz; key at right; average of two repeats).

(H) Plot of average EPSC peak amplitude for the last eight responses normalized to the first response as a function of interpulse interval (black circles). Paired-pulse recovery in the same pair (red circles).

at light-off during high-frequency stimulation that is not present in cb3 cells.

Recovery at the Cone-to-cb2 Cell Synapse

Off bipolar cells receive excitatory inputs from cone photoreceptors at dendrites in the outer plexiform layer (OPL) and inhibitory inputs from amacrine cells at axon terminals in the inner plexiform layer (IPL). Both inputs can shape the voltage response. To isolate the input from the cone synapse, cb2 bipolar cells were voltage clamped at −70 mV, which is the calculated Cl^- reversal potential, and inputs from amacrine cells were blocked by including picrotoxin and strychnine in the bath. Under these conditions, a step of light stopped a continuous inward cb2 cell current (Figure 2A and inset). Light-off was followed by an inward transient whose amplitude increased with increasing light step duration. For the bipolar cell in Figure 2A, the peak amplitude of the transient increased to a maximum with a time constant, τ, equal to 90 ms. In a group of eight cb2 cells, the light-off transient displayed a rapid recovery component with τ = 72 ± 10 ms (Figure 2B). A rapid transient recovery at light-off is unique to cb2 cells insofar as the transient recoveries in cb3 (τ = 744 ± 22 ms, n = 9) and cb1 (τ = 608 ± 126 ms, n = 4) cells were uniformly

slower. We conclude that a rapidly recovering transient is already present in the cb2 cell input at the cone synapse. Moreover, since ground squirrel cones have a monophasic hyperpolarizing response to light (Figure 2, inset; Cao et al., 2014; Kraft, 1988), the synaptic transient originates in the release mechanism and not in a transient cone depolarization.

Instead of using a light step, which changes membrane voltage via a transduction cascade, the transient recovery time course can be directly measured by voltage clamping a presynaptic cone and a postsynaptic cb2 cell and then using a "two-pulse" paradigm. In this paradigm, a brief cone depolarization from −70 mV depletes a release-competent vesicle pool, while a second identical cone depolarization, given after a variable interval, determines the extent to which the pool is replenished. There is a functional similarity between the interpulse interval of the two-pulse paradigm and the duration of a light step (Figure 2, inset). We recorded cb2 cell excitatory postsynaptic currents (EPSCs) while applying two brief (1-ms) depolarizing pulses to a presynaptic cone. The strength of the cone depolarization was adjusted to produce a maximal cb2 cell response. In one experiment, the first pulse produced a peak response of approximately −440 pA (Figure 2C). After 50 ms, a second pulse produced a response of less than −30 pA, consistent with a marked depletion of the release-competent pool. For comparison, cb2 cell AMPA receptors recover from desensitization with a $\tau \approx 20$ ms (DeVries et al., 2006). As interpulse interval was increased, the amplitude of the second pulse recovered with a $\tau = 69$ ms (Figure 2D). In 35 cone-to-cb2 cell pairs, the mean recovery $\tau = 125.7 \pm 9.6$ ms (Figure 2E). Because terminal Ca^{2+} concentrations can affect the ribbon turnover rate (Babai et al., 2010), this sample of 35 cones was subdivided into cones that were depolarized for different lengths of time with different intracellular Ca^{2+} buffers, all of which had statistically similar recovery τ (Table S1). The results show that, in cb2 cells, a component of the transient response at light-off (Figures 2A and 2B) and the second EPSC response (Figures 2C–2E) recover with similarly rapid time courses.

In additional experiments, we tested for effects of receptor type and desensitization on the paired-pulse recovery. The synaptic responses of cb3 cells, which make basal contacts with cones, are mediated by both kainate and AMPA receptors (Lindstrom et al., 2014). We used UBP310 (2 μM) to isolate the AMPA-receptor-mediated component of the response. The cb3 cell paired-pulse recovery τ, 698 ± 132 ms (n = 6 pairs), was significantly slower than that measured at the cone-to-cb2 cell synapse ($p < 0.0001$, unpaired t test), suggesting that the slow recovery of the light-off response in cb3 cells is not due solely to kainate receptor expression. Recovery was also measured in control and cyclothiazide (CTZ) containing solutions. CTZ increases AMPA receptor affinity and relieves desensitization (Patneau et al., 1993). Paired-pulse recovery τ and maximal EPSC amplitudes were unchanged in CTZ (Table S2), while the maximal EPSC response width at half-height was significantly increased (4.2 ± 0.9-fold; paired t test, $p = 0.014$). The results show that the rapid recovery τ at the cone-to-cb2 cell synapse is not an outcome of receptor desensitization. In addition, the combination of maintained EPSC amplitude and extended duration may signify that receptor saturation occurs in CTZ.

Frequency Dependence of Synaptic Depression

To determine whether rapid replenishment is maintained during multiple cycles of release that are predicted to deplete the entire ribbon-associated pool (Babai et al., 2010; Bartoletti et al., 2010), a cone was stimulated in the loose seal configuration with a train of 1-ms pulses at varying frequencies (Figures 2F and 2G). An initial 1-ms cone depolarization produced a maximal EPSC in a postsynaptic cb2 cell. We assume that each depolarization depletes the pool of release-competent vesicles and that replenishment takes place during the interval between depolarizations. At rates of 1–4 Hz, all EPSC amplitudes were similar. At rates of 8–64 Hz, the peak response amplitude declined after the initial pulse but quickly reached a steady level. A plot of normalized EPSC amplitude (average of the last eight responses) relative to the first EPSC response was fitted with an exponential curve that had a $\tau = 110$ ms, similar to the τ obtained from a two-pulse experiment in the same pair ($\tau = 75$ ms; Figure 2H). Comparable results were obtained from six cone-to-cb2 cell pairs (paired pulse $\tau = 91.1 \pm 12.8$ ms versus pulse frequency $\tau = 137.6 \pm 45.1$ ms; values are not statistically different by a paired t test; $p = 0.058$). We conclude that recovery at the cone-to-cb2 cell synapse occurs with a τ of about 130 ms, which is equivalent to a 37% reduction in transient peak amplitude at a frequency of ~7.5 Hz. This reduction in peak amplitude, which occurs during both pulse pairs and longer trains, is similar to the decrease in the cb2 transient amplitude during square wave light at 8 Hz (Figures 1A, 1C, and 1D).

The Time Course of Presynaptic Recovery

The 130-ms recovery τ, if attributed to presynaptic vesicle replenishment, implies a steady vesicle fusion rate of ~3,100 s^{-1} (1/0.13 s × 400 docking sites per cone). This value greatly exceeds the measured release rates in salamander (~500 vesicles-s^{-1}; Sheng et al., 2007), lizard (~400; Choi et al., 2005), and ground squirrel (~1,000; DeVries et al., 2006) cones. To determine whether the postsynaptic recovery τ accurately represents the presynaptic replenishment τ, we modified the paired-pulse experiment so that we could simultaneously measure the EPSC and the H^+ block of the Ca^{2+} current (DeVries, 2001). At bipolar cell ribbons, the H^+ block of the Ca^{2+} current is proportional to the amount of vesicle fusion, as shown by capacitance measurements (Palmer et al., 2003). The cb2 EPSC was measured during two 15 ms steps from −70 to −30 mV (Figure 3A, upper traces) and recovered with $\tau = 50$ ms (Figure 3B, red circles). The H^+ block of the cone Ca^{2+} current was measured during the same series of pulses as the first step response minus the second (Figure 3, inset; DeVries, 2000). At short interpulse intervals, when only a small fraction of the presynaptic vesicle pool is recharged, the H^+ block was small or absent during the second pulse and the cone difference current was maximal (Figure 3A, lower traces). With increasing interpulse interval, the H^+ block recovered so that the shape of the current during the second pulse approached that of the first pulse and the difference current became smaller. In the plot shown in Figure 3B, the H^+ block recovered with a $\tau = 410$ ms. In a total of six pairs (Figure 3C), the recovery τ for the cb2 EPSC response (98 ± 21 ms) was faster than that of the H^+ block (332 ± 57 ms; significantly different at $p = 0.0094$; paired t test). In a larger

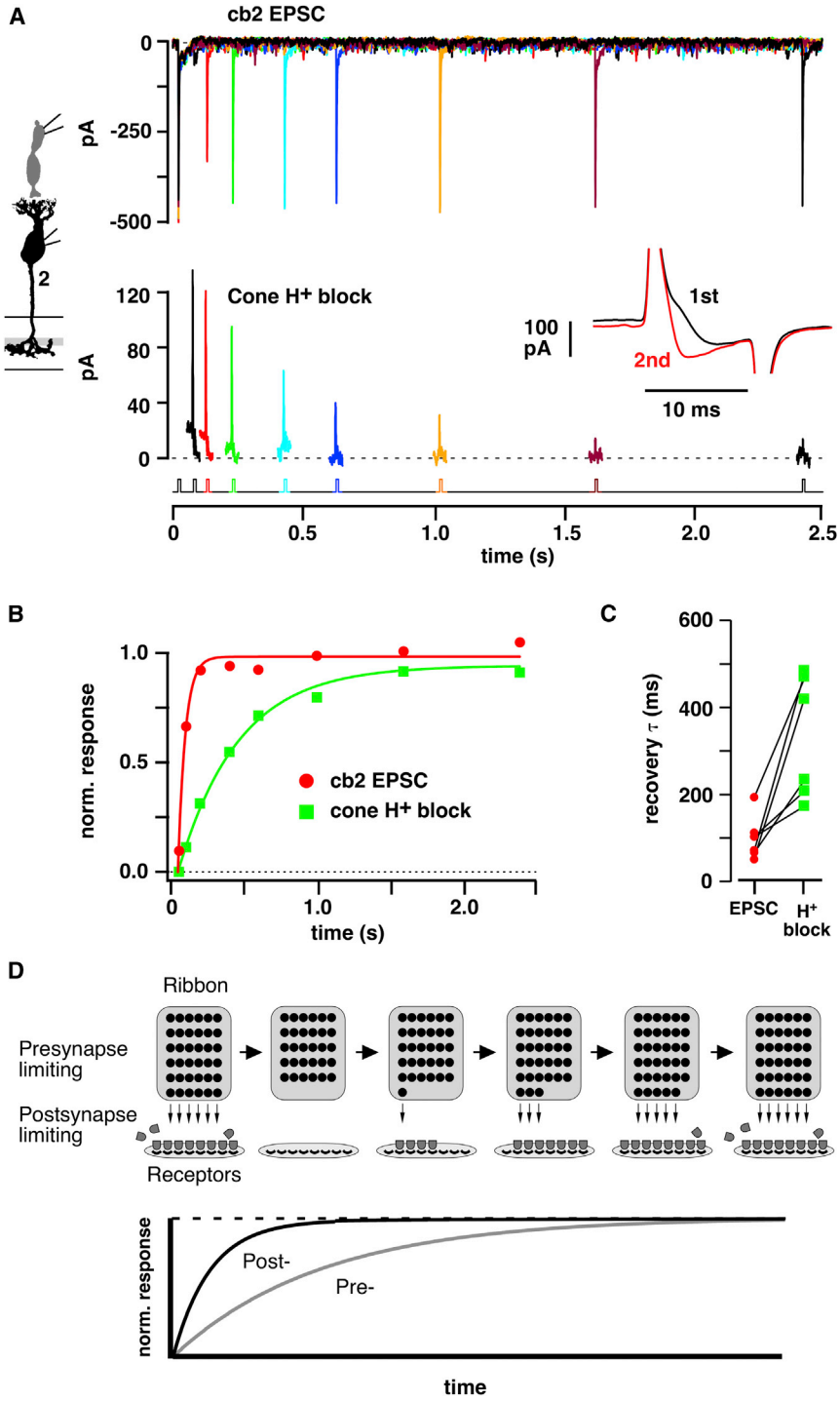

Figure 3. Simultaneous Measurement of H^+ Block and cb2 EPSC Recovery

(A) Upper panel: paired-pulse response in a cb2 cell during 15-ms cone steps from −70 to −30 mV. Lower panel: H^+ block measured as the difference between the current during the first and second steps. With increasing interpulse interval, the H^+ block during the second pulse more closely approximates that of the first and the difference current becomes smaller. Inset: pair of cone step currents separated by a 50-ms interval. The difference current equals the first trace minus the second.

(B) Plot of normalized (norm.) recovery versus interpulse interval.

(C) Pre- and postsynaptic recovery time constants. Lines connect simultaneous measurements (n = 6 pairs).

(D) Mechanism of fast postsynaptic recovery. After an initial brief depolarization that releases the vesicles docked in the first ribbon row, new vesicles dock and become competent to fuse over time (rightward progression indicated by arrows illustrating the case where the presynaptic recovery is limiting). A second pulse releases the contents (convex shapes) of newly competent vesicles. Postsynaptic recovery can be limiting under conditions where transmitter concentrations are high and receptors saturate before the presynapse fully recovers.

sample of cones that were not paired with a cb2 cell, the recovery from proton block occurred with a τ = 448.7 ± 28.2 ms (n = 58). Subsets of cones were recorded in HEPES buffer (5 mM) to reduce the likelihood of proton block saturation (τ = 474.9 ± 43.8 ms; n = 16), in DL-*threo*-β-benzyloxyaspartic acid (TBOA; 100–200 μM) to block the activation of a transporter anion conductance by released glutamate (τ = 470.6 ± 35.7 ms, n = 43), and during β-escin-perforated patch recordings that minimized rundown (τ = 556.2 ± 83 ms, n = 11; differences were not significant at the $p < 0.05$ level; Wilcoxon rank-sum test; recovery in some cones was measured under several conditions). The results suggest that the cb2 cell EPSC recovers faster than the cone release-competent vesicle pool, a mismatch that can occur if receptor saturation limits the size of the postsynaptic response so that a partial presynaptic recovery is associated with a full postsynaptic recovery (Figure 3D).

Relationship between EPSC Amplitude and Cone Membrane Capacitance Change

To better compare the time courses of presynaptic vesicle replenishment and postsynaptic EPSC recovery, we simultaneously measured cone membrane capacitance (C_m) and cb2 cell EPSC response. We first confirmed in a two-pulse experiment that replenishment at the cone terminal is relatively slow. Two examples (Figures 4A and 4B) show depolarization-evoked C_m jumps of 15.0 and 13.2 fF preceding intervals of 200 and 500 ms, respectively. After the intervals, a second step led to smaller jumps of 6.5 and 6.6 fF, respectively. Changes in membrane (G_m) and pipette (G_s) conductance, that can obscure changes

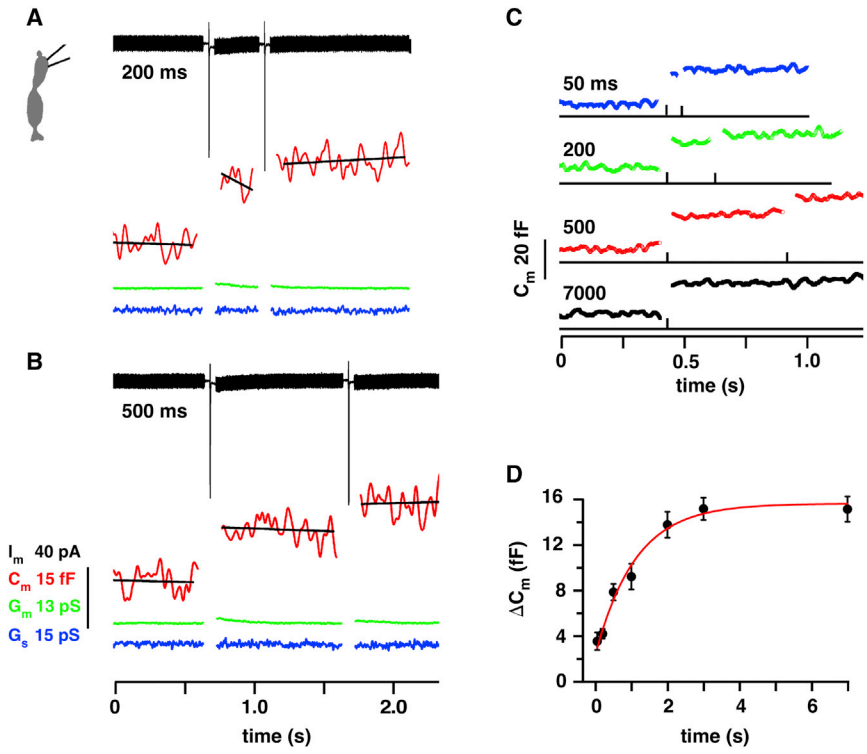

Figure 4. Cone Membrane Capacitance Change as a Function of Interpulse Interval

(A) ΔC_m was measured before and after 1-ms steps separated by 200 ms. A thick membrane current trace (I_m, black) is produced by the response to the sinusoidal voltage command. The sharp inward deviations result from Ca^{2+} current activation during the 1-ms steps. The Lockin parameters were: membrane conductance (G_m, green trace), C_m (red trace), and series conductance (G_s, blue trace). The capacitance traces were fitted with a straight line to determine the average value.

(B) Same as in (A), but with a 500-ms interval. Steps were from −70 to −10 mV. Scale bars apply to (A) and (B).

(C) Average ΔC_m responses for the interpulse intervals at left (n = 6 cones).

(D) Plot of ΔC_m during the second pulse versus interpulse interval. Data were not normalized, since the responses to the first jump were similar. The recovery τ was 1.11 s (red curve). Including zero in the fit produced a τ = 0.70 s (data not shown).

in C_m, were not observed. Average responses (Figure 4C; n = 6 cones) were used to plot ΔC_m versus interpulse interval (Figure 4D), which was fitted with a saturating exponential to give a τ of 0.7–1.1 s. Thus, the cone C_m replenishment τ was slower than the recovery τ for EPSCs and comparable to that obtained by measuring the H^+ block.

If receptor saturation limits EPSC amplitude, then a range of depolarizing stimuli should increase cone transmitter release without concomitantly increasing cb2 cell EPSC amplitude. To identify this range, we compared presynaptic capacitance jumps to postsynaptic EPSC responses during paired recordings (Figure 5). To generate a variety of response amplitudes, we depolarized the cone with a pair of 1-ms pulses separated by an interval of 500 ms, which is slightly less than the τ for cone recovery. The first pulse was either to −40, −30, −10 or +30 mV, and sometimes released only a portion of the presynaptic pool, and the second pulse was always to −10 mV. EPSCs differed in amplitude but not shape (Figure 5B), so we used amplitude as a measure of response strength. ΔC_m and corresponding peak EPSC amplitudes were individually compared. Figure 5A shows the results from a single pair. In this experiment, the largest individual ΔC_m and EPSC responses, ~20 fF and approximately −400 pA, were obtained during steps to −10 mV that were either first in the sequence or second and not preceded by an EPSC response. On average, first steps to −10 and +30 mV produced the largest capacitance jumps, with ΔC_m values of 15.0 ± 1.4 and 13.3 ± 1.9 fF (n = 9 pairs), respectively. Corresponding EPSCs were −382 ± 21 and −366 ± 20 pA. A step to −30 mV elicited a much smaller capacitance jump (2.3 fF) and a still substantial EPSC of −253 pA (Figure 5A). Overall, steps to −30 mV elicited a 5-fold smaller than maximum ΔC_m, 2.2 ± 0.3 fF, and a peak EPSC response of −179 ± 31 pA, which was only 2-fold smaller than that obtained during the steps to +30 and −10 mV.

A plot of EPSC amplitude versus ΔC_m (Figure 5C) obtained from the pair shown in Figure 5A showed a steep increase in peak current as a function of ΔC_m in the range of 0–5 fF. For larger capacitance jumps, EPSC amplitude leveled off. The plot in Figure 5D summarizes results from nine cone-to-cb2 cell pairs. By ~2 fF, the EPSC had reached half-maximal saturation, and by ~5 fF, the response was 80% of its maximum. An average maximal capacitance jump of 15 fF corresponds to roughly 15 vesicles fusing per ribbon (assuming 0.05 fF per vesicle [Neef et al., 2007] and ~20 ribbons per terminal [Li and DeVries, 2006]), while 50% and 80% EPSC responses correspond to two and five fused vesicles per ribbon, respectively. The results show that AMPA receptors at the cone-to-cb2 cell synapse saturate during a strong cone stimulus.

A Weak Antagonist Relieves Receptor Saturation at the Cone-to-cb2 Cell Synapse

Weak competitive antagonists allow receptors to respond to increases in glutamate concentration at levels that would normally be saturating (Chanda and Xu-Friedman, 2010; Diamond and Jahr, 1997; Neher and Sakaba, 2001; Wadiche and Jahr, 2001). Paired-pulse recovery was measured both in control and in a weak antagonist-containing solution (kynurenic acid [KYN] 1–4 mM). KYN (2 mM; Figures 6A and 6B) reduced the maximal EPSC amplitude by 50% and prolonged the cb2 cell EPSC recovery time course (τ = 426 versus 155 ms; Figure 6C). Pairwise comparisons (Figure 6D) showed a statistically significant 3.9 ± 1.3-fold increase in recovery τ (KYN versus control, n = 4 pairs, p = 0.02; paired t test; τ = 135 ± 25 ms in control and 440 ± 60 ms in KYN). Critically, the EPSC amplitudes in KYN continued to increase at interpulse intervals where the

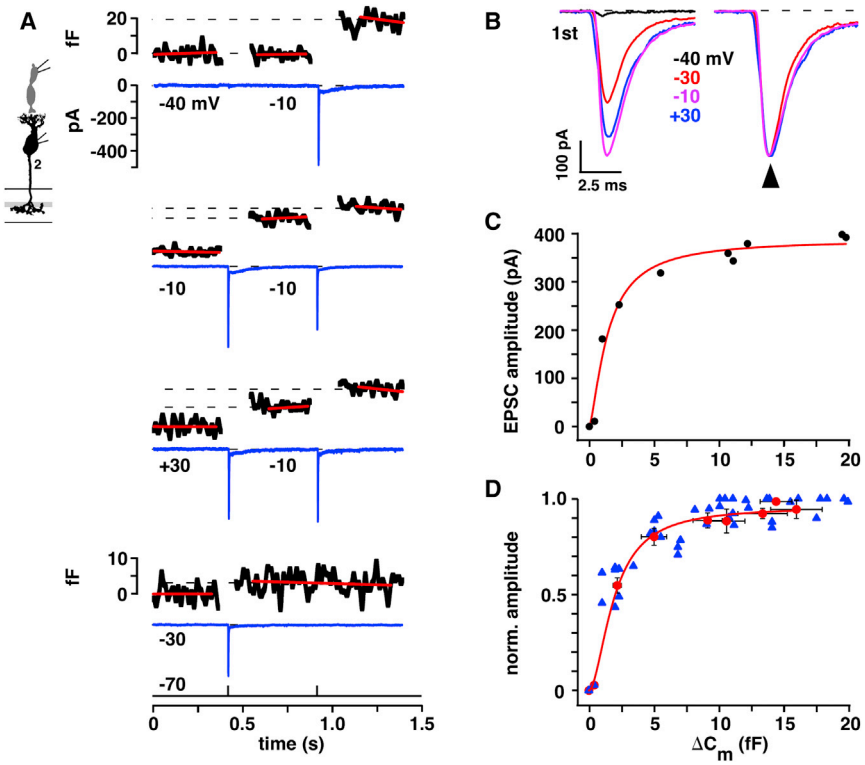

Figure 5. A Saturating Relationship between Cone ΔC_m and cb2 Cell EPSC Amplitude

(A) Responses from a cone-to-cb2 cell pair. For each set of cone pulses, cone ΔC_m is plotted above and baseline-subtracted cb2 cell current is plotted below. Step voltage (from −70 mV) is indicated below the current trace prior to the corresponding 1-ms pulse. Capacitance and membrane current scales apply throughout except where indicated. The lowermost set of traces contains a single step to −30 mV.

(B) cb2 cell EPSC responses during cone pulses to between −40 and +30 mV (left) are shown normalized (right). With the exception of the smallest response, which did not have a corresponding ΔC_m, the responses peaked at the same time (arrow).

(C) Plot of EPSC amplitude versus ΔC_m for the pair in (A). EPSC amplitude attained 90% of its maximal value when ΔC_m was ~10 fF (Hill fit: R_{max} = 388 pA, $\Delta C_{m(1/2)}$ = 1.44 fF; n = 1.42, r^2, = 0.97).

(D) Peak EPSC response is plotted against ΔC_m. Blue triangles show responses during each pulse across all pairs regardless of pulse voltage. Responses were normalized by the largest EPSC peak amplitude. Red circles replot the data where responses were first normalized to the maximum value in a pair and then averaged across pairs according to the amplitude of the voltage step, distinguishing between responses obtained during the first and second pulses (Hill fit: $\Delta C_{m(1/2)}$ = 2.3; n = 2, r^2 = 0.99). The red curve is fitted to the red circles.

recovery in control had neared its maximum value (Figures 6A–6C). Between 0.4 and 1.0 s, the second EPSCs in KYN increased by 46.9% ± 12.0%, while the corresponding EPSCs in control increased by only 7.3% ± 2.0% (significantly different by unpaired t test; p = 0.017). An increase in the EPSC amplitude in the presence of a weak antagonist without a comparable increase in control is consistent with the relief of receptor saturation.

Next, we used KYN to examine whether receptors saturate during a light response. For these experiments, we compared the effect of 1 mM KYN on the amplitudes of the light-off transients after 0.2- and 1.0-s steps. We chose these pulse intervals because they were associated with similar amplitude EPSCs in control (Figure 2A) but might produce different peak glutamate concentrations based on the τ for refilling of the cone vesicle release pool. In one cb2 cell, the average control light-off EPSC amplitude increased by 2% between the 0.2- and 1.0-s pulses, whereas the EPSCs in KYN increased by 2.8-fold (Figure 6E, upper panel). A small increase in the amplitude of the control EPSC accompanied by a large change in the amplitude of the EPSC in KYN is consistent with receptor saturation during the second light-off response. Similar results were obtained in a total of six cells where the amplitude ratios of the first and second EPSCs in control were not significantly different ($EPSC_{0.2}$ = −168.5 ± 15.6 pA; $EPSC_{1.0}$ = −216.6 ± 31.7 pA, p = 0.10; paired t test). In the same cells (Figure 6F), KYN reduced the size of the light-off transient following a 0.2-s step by 63.5% ± 5.7% (−60.3 ± 9.5 pA versus −168.4 ± 15.6 pA; p = 0.0001), but it did not affect the EPSC amplitude following a 1-s light step (−220.9 ± 35.7 pA versus −216.6 ± 31.7 pA; p = 0.86). The peak current blocked by KYN was also significantly different between the 0.2- and 1.0-s pulses (p = 0.0009). As a control, we presented the same light steps in the presence of CNQX (0.4 μM), a strong AMPA receptor antagonist that should reduce the amplitude of the transient by the same amount regardless of light duration. In an individual recording, CNQX suppressed the light-off transient by 53% and 61% after the 0.2- and 1.0-s steps, respectively (Figure 6E). In nine recordings, transient amplitudes in CNQX were reduced by 41.2% ± 5.5% and 34.4% ± 7.9% following 0.2- and 1.0-s steps, respectively (p values for 0.2- and 1.0-s flashes different from control = 0.0005 and 0.007, respectively; p for 0.2- and 1.0-s flashes different from each other = 0.177; Figure 6F). The results are consistent with the idea that the glutamate concentrations at cb2 cell receptors approach saturation during the transient that follows a 1.0-s light pulse.

Monte Carlo Simulation of Transmission

We used a Monte Carlo simulation (Stiles and Bartol, 2001) to investigate the relationship between the number of transmitter quanta released at a ribbon and the saturation of cb2 cell AMPA receptors. The first task was to specify synapse geometry (Figures 7A and 7B; Figure S1). Importantly, we chose a ribbon-base length of 750 nm from a range of 200–1,000 nm (Sterling and Matthews, 2005). An electron microscopy (EM) reconstruction of a cone ribbon with a similar length docked 36 vesicles (Sterling and Matthews, 2005). The kinetic model describing the cb2 receptor response to glutamate was modified from Häusser and Roth (1997). Specifically, the rate constants

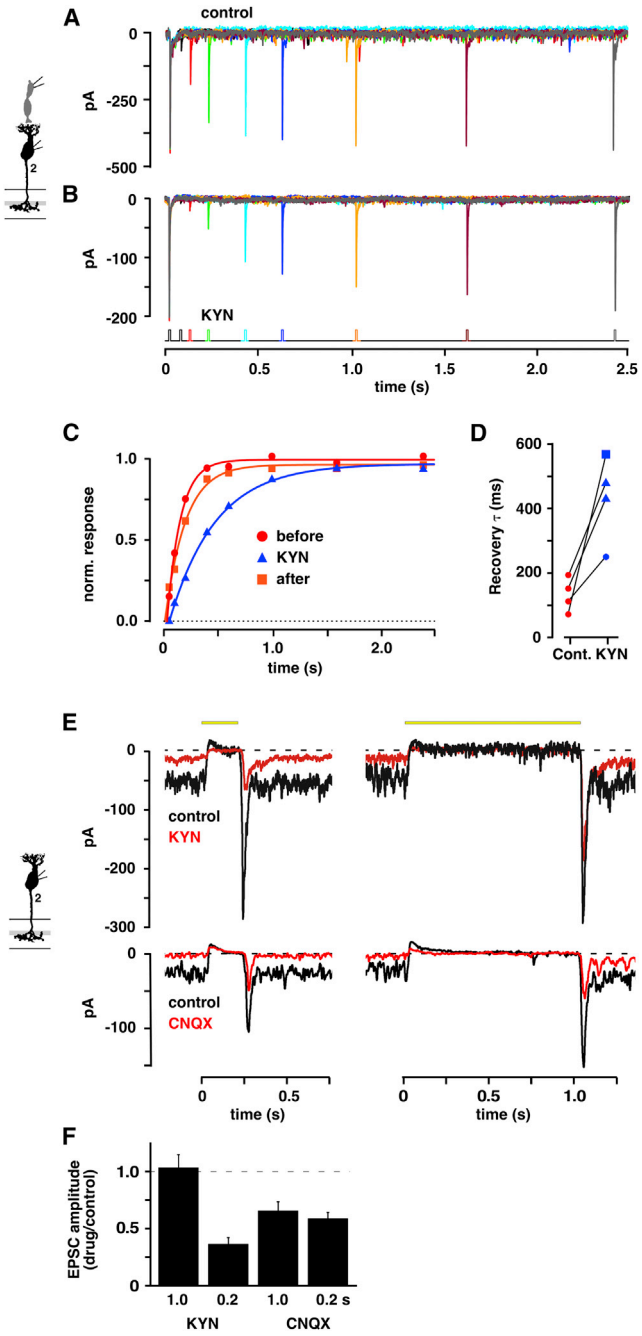

Figure 6. Weak Antagonists Relieve Receptor Saturation at the Cone-to-cb2 Cell Synapse

(A and B) A cone was depolarized from −70 to −30 mV for 15 ms in whole-cell voltage clamp. Paired-pulse recovery of the EPSC response was measured in (A) control and then in (B) a 2-mM KYN-containing solution.

(C) Normalized (norm.) recovery versus interpulse interval in control (red circles) and 2 mM KYN (blue triangles).

(D) Recovery τ in control and KYN with results from the same pair connected (KYN: blue square = 4 mM; blue circle = 1 mM). The τ in control is an average of before and after treatment. Decreased amplitude (%) in KYN from top to bottom equaled 65.7, 61.3, 50.8, and 29.4.

(E) Light responses in control and 1 mM KYN- (upper) or 0.4 μM CNQX (lower)-containing solution during steps of either 0.2 or 1.0 s (light intensity = 3.0×10^6 photons-μm^{-2}-s^{-1}; rows show responses from the same cell; traces are averages).

(F) Histogram of EPSC amplitude in drug (KYN, n = 6; CNQX, n = 9) divided by control solution for the two light step durations.

involving glutamate binding were increased to account for a small difference in EC_{50} (half maximal effective concentration) between cb2 and Purkinje cell AMPARs (340 versus 440 μM, respectively (DeVries et al., 2006; Häusser and Roth, 1997; Figure S2). We tested the simulation by releasing a single vesicle at a distance of 180 nm (DeVries et al., 2006) from the model cb2 receptor array and then comparing the time course of simulated and actual small EPSCs. The simulated glutamate concentration at the receptor array peaked at 500 μM, 25 μs after release. The actual and simulated EPSC time courses were similar with the largest deviations occurring during the response decay (Figure S3). Next, we simulated the simultaneous release of 1–36 docked vesicles. A plot of normalized EPSC amplitude versus the number of released vesicles (Figure 7C) showed saturation for invaginating but not basal contacts. The cb2 cell EPSC response was ~50% saturated when 2.5 vesicles were released, matching the capacitance results. We varied the number of glutamate molecules per vesicle (2,000–5,000) and the transmitter diffusion constant (0.1–1.0 cm^2-s^{-1}) and found that saturation was robust to these uncertainties (Figure S4).

To more closely approximate conditions during a light response, we released vesicles with temporal jitter. We selected vesicle release times according to a probability distribution derived from the rising phase of the cone Ca^{2+} current (Figure S5). The resulting simulated EPSCs had a time course similar to our light response data (Figure 7D). With the increased release spread, the maximal response occurred at higher vesicle numbers, but a 50% maximal response was still achieved with fewer than five released vesicles (Figure 7E), and receptors approached 80%–90% of their saturated response when 20–25 vesicles per ribbon were released. The simulations support the idea that cb2 receptors display a saturating non-linearity under both experimental and physiological conditions.

DISCUSSION

The perception of a rapidly changing visual stimulus is limited by the frequencies signaled at the cone synapse. Primate horizontal and ganglion cells can process 80–100 Hz flicker (Derrington and Lennie, 1984; Smith et al., 2001), but moderate (~0.2 Hz) rates of vesicle refilling of the release pool at the cone ribbon motivated us to address the question: how do cone ribbons signal high temporal frequencies to postsynaptic bipolar cells?

Behavioral and functional tests in the ground squirrel suggest that the sensitivity to high-frequency flicker equals or exceeds that in humans (Jacobs et al., 1980; Tansley, 1965). Correspondingly, ground squirrel cone light responses are 30%–50% faster than those of primate cones (Cao et al., 2014; Kraft, 1988). The bipolar cells that mediate high-frequency signaling in the ground squirrel retina have not been identified, but the cb2 cell is a candidate. The cb2 cell stands out because it has a transient depolarization at light-off that exceeds the baseline voltage at 16 Hz and is still prominent at 32 Hz (Figure 1). Additionally,

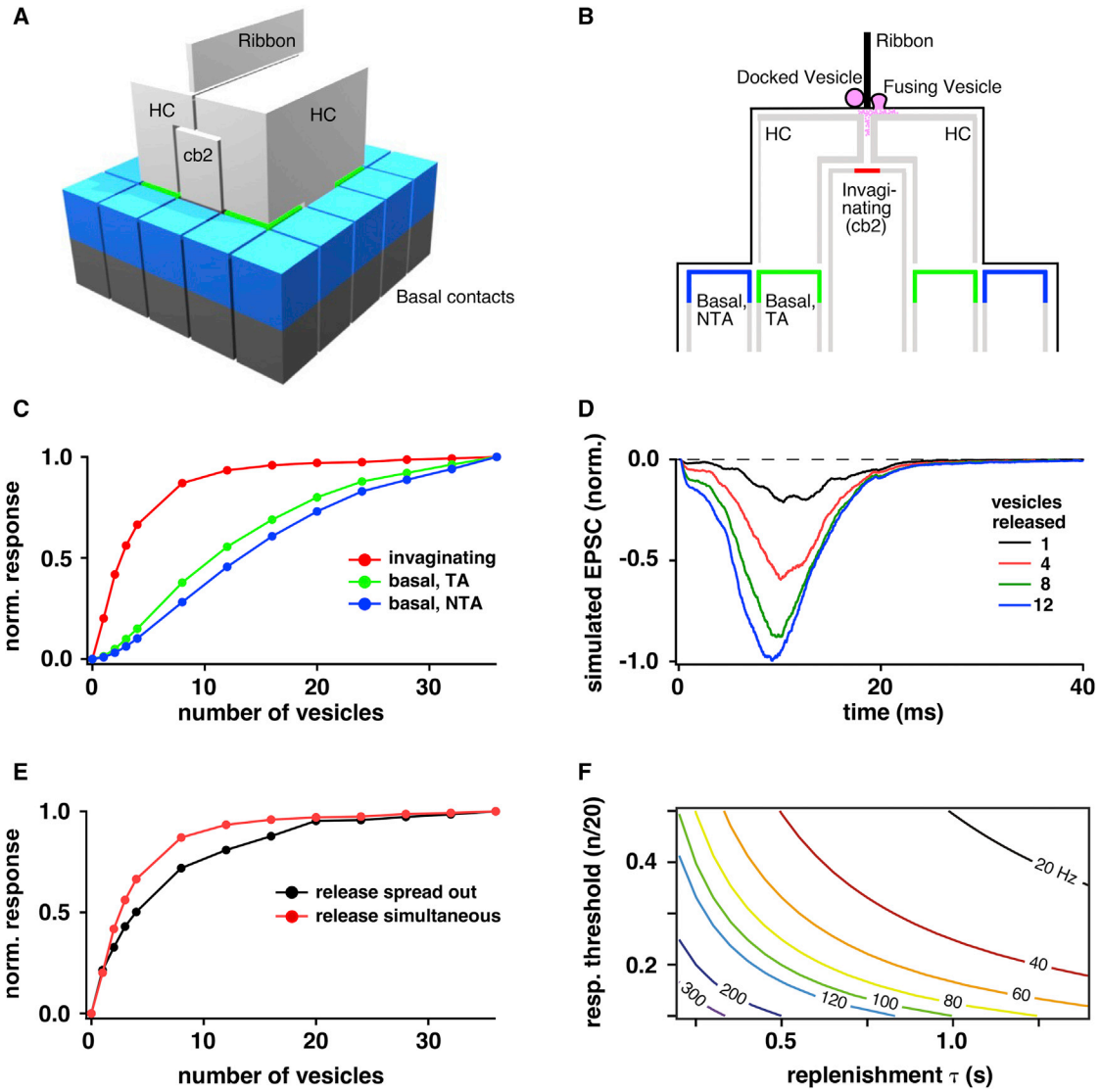

Figure 7. Monte Carlo Simulation

(A) The model contains a synaptic ribbon, two invaginating horizontal cell (HC) processes, an invaginating bipolar cell process (cb2), and contacts at basal postsynaptic locations (blue and green). The cone membrane is omitted for clarity.

(B) A cross-section illustrates the relationship between ribbon docking sites, the synaptic cleft including the cone membrane (thin black line), and the location of postsynaptic receptors, 180 (red) or >500 nm (green and blue) below the release sites. Basal contacts are designated as triad associated (TA) or non-TA.

(C) Normalized (norm.) EPSC amplitude versus number of released vesicles for the three different contact locations during synchronous release.

(D) Simulated EPSCs incorporating release jitter. The 20%–80% rise time of the 12-vesicle response was 4.25 ms. For comparison, the rise time of the transient current response at light-off following a long step is 6.86 ± 0.33 ms and potentially includes variability in the light response among cones.

(E) Normalized EPSC amplitude versus number of vesicles released for synchronous versus temporally spread release.

(F) Predicted maximum signaling frequency (numbers on selected plots) as a function of response threshold and vesicle replenishment τ (see Discussion).

See also Figures S1–S5 and Supplemental Experimental Procedures.

cb2 cells have dendrites that are close to the sites of ribbon-mediated transmitter release within invaginations (DeVries et al., 2006); express AMPA receptors that recover rapidly from desensitization (τ = ~20 ms; DeVries, 2000); and contain the GluA4 subunit (Lindstrom et al., 2014), which is associated with rapid transmission (Koike-Tani et al., 2005). On investigating the interval dependence of the transient response at the cone-to-cb2 cell synapse, we found a paradoxical difference between the time courses of presynaptic refilling and postsynaptic recovery. The postsynaptic recovery τ was 130 ms (Figure 2), whereas the presynaptic replenishment τ was 500–1,000 ms (Figures 3 and 4). Simultaneous cb2 cell EPSC and cone capacitance measurements resolved this paradox by showing that the coordinated fusion of cone vesicles could produce postsynaptic

receptor saturation (Figure 5), consistent with a Monte Carlo model (Figure 7). Experiments with a weak antagonist further suggested that saturation can occur following a light stimulus (Figure 6) and acts to speed up the apparent recovery time course of the Off transient (Figure 2). Hence, by limiting the dynamic range of signaling, the cone-to-cb2 cell synapse counteracts ribbon depression.

Alternative Mechanisms for the Rapid Recovery of the cb2 Cell Transient

The Off cone bipolar cell types have different temporal light responses (Baden et al., 2013; Ichinose and Hellmer, 2015). These differences can originate from the cone synapse (DeVries, 2000), from voltage-dependent currents in the bipolar cell membrane (Ichinose et al., 2005; Ma et al., 2005; Puthussery et al., 2013; Saszik and DeVries, 2012), from inhibitory inputs at the bipolar cell terminal (Eggers and Lukasiewicz, 2011), or from a combination. The rapid recovery that we demonstrate originates in a specialized mechanism at the cone synapse since it persists when the bipolar cell is voltage clamped and bathed in drugs that block amacrine cell synapses. In current clamp without blockers, the transient at light-off may be enhanced or shaped by a momentary gap in inhibition at amacrine to bipolar cell synapses in the inner retina (Dong and Werblin, 1998; Lagnado, 1998). In addition, transient Off bipolar cell types in the mouse (Ma et al., 2005; Baden et al., 2013) and primate (Puthussery et al., 2013), but not the ground squirrel (Saszik and DeVries, 2012), express a voltage-dependent Na^+ current or another transient generating mechanism (Baden et al., 2013) that may amplify the responses at the cone synapse. Taken together, these results suggest that a combination of mechanisms may support high-frequency signaling in certain Off bipolar cells.

Relationship between Synapse Saturation, Gain, and Frequency Response

For small cone depolarizations, the cb2 cell synapse has a relatively steep relationship between the number of released vesicles and the EPSC response (Figure 5). We extended our model to further examine the signaling function of this high-gain region of the input-output curve. A simple model assumes a square wave light stimulus with a high cone release rate in the dark, zero release in bright light, and a τ that characterizes the refilling of the docked pool of vesicles during the half period in bright light. The model further assumes that there are 20 vesicle docking sites per ribbon and that n repopulated vesicle sites undergo synchronous release at light-off. For the model to be useful, we need to posit a bipolar cell threshold for transmitter release onto ganglion cells followed by an estimate of how many cone vesicles must be released at light-off in order to depolarize the bipolar cell to threshold. We assign a bipolar cell threshold of 2–3 mV relative to the resting level in bright light and estimate from the light response amplitude (30.7 mV; Figure 1A) and the input-output curve ($\Delta C_{m(1/2)}$ equivalent to 2.3 vesicles per ribbon; Figure 5D) that bipolar cell threshold is reached when n equals 0.3–0.45 vesicles per ribbon (see Supplemental Experimental Procedures).

The highest temporal frequency signaled in bright light, f_{Max}, corresponds to the time that recharges just enough vesicles per ribbon, n, to produce a threshold response in the bipolar cell. We can relate $n/20$ to f_{Max} by

$$f_{Max} = \left(-2\,\tau\,\ln\left(1 - \frac{n}{20}\Big|_{Threshold}\right)\right)^{-1}.$$

The maximum signaling frequency increases by reducing the response threshold, n, equivalent to an increase in gain, or by decreasing the vesicle refilling τ. Using a replenishment τ = 0.7 s and an n = 0.30–0.45, we arrive at an f_{Max} = 31–47 Hz. This frequency range is likely an underestimation, because it relies on average values that might include cells whose synaptic responses have started to run down during whole-cell recording. If, instead, we use the $\Delta C_{m(1/2)}$ value from the experiment shown in Figures 5A–5C, which is equivalent to 1.44 vesicles per ribbon (equal to 0.19–0.28 vesicles per ribbon at threshold) and a replenishment τ of 0.5, representative of the τ obtained from proton block measurements, then f_{Max} = 70–105 Hz. The relationship between f_{Max}, response threshold, and replenishment τ is plotted in Figure 7E over the range of interest for the cone synapse. Several observations favor the higher frequency range: the amplitude of the 32-Hz square wave response (Figure 1A) was 7.6 ± 0.5 mV, substantially greater than the benchmark 2–3 mV threshold; the synapse itself can signal frequencies exceeding 64 Hz (Figures 2F and 2G); and a light-off transient recovery τ = 90 ms (Figure 2A) is equivalent to a frequency of 54–82 Hz, assuming a threshold of 2–3 mV and a 30.7-mV peak response. Alternatively, if the frequency range of the individual bipolar cell is, indeed, lower than the behavioral or ganglion cell limit, summation in the inner retina at the bipolar-to-ganglion cell synapse may extend the perceptual range to higher frequencies. While containing some uncertainties, our simple model shows how a high-gain synaptic response can encode a high-frequency light stimulus. Examined from the point of view of high-frequency transmission, synapse saturation at low frequencies is an outcome of building a high gain synapse.

Receptor Saturation during a Physiological Stimulus

cb2 cell receptors saturate when vesicles are synchronously released during a cone step in voltage clamp (Figure 5). However, cone depolarization after a light pulse has a relatively slow rise time (~5 ms) that should produce a staggering of vesicle release and a reduction of the peak glutamate concentration. We used a weak antagonist, KYN, to investigate saturation during a light response. In paired recordings, KYN increased the recovery, τ, from an average of 135 to 440 ms. A prolonged recovery time course, especially at long interpulse intervals when the control EPSC has reached a steady level, is consistent with relief from receptor saturation. EPSC responses following light steps of 0.2 and 1.0 s had similar amplitudes in control but were also differently blocked by 1 mM KYN (Figures 6E and 6F), consistent with a prolongation of the recovery τ and saturation following the 1.0-s step. Weak antagonists such as KYN effectively reduce the affinity of the receptor for glutamate, allowing the receptor to respond to concentrations that would normally be saturating. This effect of KYN is concentration dependent: the recovery τ should be nearly unchanged (i.e., 135 ms) in very low concentrations of KYN insofar as saturation

still occurs. In relatively high concentrations of KYN, the recovery τ should approach the presynaptic refilling τ (0.7–1.1 s). The measured τ in 1–4 mM KYN, 440 ms, is in the middle of this range. By relieving saturation and prolonging the recovery time course, KYN lengthens the time required for the postsynaptic response in the bipolar cell to reach threshold for release onto postsynaptic ganglion cells, thereby reducing the frequency bandwidth of the pathway.

Our results supporting AMPA receptor saturation during light differ from those at the rod bipolar to AII amacrine cell synapse (Dunn and Rieke, 2008) but are similar to those at the bipolar-to-ganglion cell synapse (Chen and Diamond, 2002; Sagdullaev et al., 2006). A different type of saturation occurs at the rod-to-rod bipolar cell synapse during steady glutamate release in the dark. At this synapse, saturation occurs within a G protein cascade that links metabotropic glutamate receptors to membrane ion channels, introducing a threshold non-linearity (Sampath and Rieke, 2004).

Versatile Processing at Retinal Ribbons

A recent idea is that retinal ribbon synapses are versatile processing units that can perform different functions depending on the wiring of their local circuit. The key to this versatility is the causal link between tonic replenishment and phasic release. Depression at bipolar cell ribbons plays a role in luminance and contrast adaptation (Kastner and Baccus, 2014; Oesch and Diamond, 2011) and in encoding the full 10–12 log units of intensity, over which natural stimuli vary (Euler and Masland, 2000; Kastner and Baccus, 2014; Singer and Diamond, 2006). In these roles, the fraction of docking sites that contain release-competent vesicles is adjusted to maintain coding efficiency while avoiding saturation in the signaling pathway. Even when AMPA receptor saturation occurs at the "On" bipolar-to-ganglion cell synapse, NMDA receptors are recruited to maintain the dynamic range (Chen and Diamond, 2002; Sagdullaev et al., 2006). Our results also rely on the causal link between tonic replenishment and phasic release but illustrate an opposing idea, which is that saturation at cb2 cell contacts can improve temporal performance at the expense of dynamic range and coding efficiency.

Versatility is also characteristic of the cone synapse, where a single output provides input to as many as 14 bipolar cell types, a number of which have distinctive temporal responses. Indeed, a recent study in the mouse (Kim et al., 2014) shows how a subtle interplay between transient and sustained bipolar cell responses can produce directional responses in starburst amacrine cell neurites. In their model, a sustained bipolar cell such as the mouse type 1 or 4 or the ground squirrel cb3 makes axonal contacts with the central regions of a starburst cell's neurites, while transient responding bipolar cells, such as the mouse type 3a or 3b and the ground squirrel cb2, contact starburst cell processes more peripherally. The result is that a centrifugally moving bar of light creates a temporal sequence of excitatory inputs that reinforce each other along the neurite, eliciting transmitter release from the neurites tips onto the dendrites of directionally selective ganglion cells. This model illustrates how the high-frequency transients at the cone-to-cb2 cell synapse may interact with more sustained bipolar cell responses to bring about complex temporal processing in the inner retina.

In the mammalian retina, the majority medium/long-wavelength-sensitive cones provide input to almost all of the bipolar cell types. A high vesicle replenishment rate at the cone photoreceptor synapse in the dark would ensure that all types can signal at the highest temporal frequencies but with a metabolic cost. However, most ganglion cell types do not carry high-frequency information (Baden et al., 2016); thus, the metabolic cost can be lowered by reducing the ribbon replenishment rate while, at the same time, creating specialized synaptic contacts that can convey and amplify high-frequency components at the expense of dynamic signaling range.

EXPERIMENTAL PROCEDURES

Preparation and Electrophysiology

Procedures were approved by the Northwestern University Animal Care and Use Committee. The procedure for making ground squirrel (*Ictidomys tridecemlineatus*) retinal slices has been described previously (DeVries et al., 2006; DeVries and Schwartz, 1999). For experiments involving light responses, retinal slices were obtained under dim red illumination (Saszik and DeVries, 2012) and visualized under infrared illumination with a Zeiss Axioskop-2FS microscope using a 63× water immersion objective. Recordings were made with Axopatch 200B amplifiers (Molecular Devices). Signals were filtered at 5 kHz and digitized at 10 kHz with a HEKA ITC-18 (HEKA Elektronik) operated with custom software (Igor Pro 6.1; WaveMetrics). Patch pipettes were pulled from borosilicate glass capillary tubes to tip resistances of 8–12 MΩ.

The external solution consisted of the following (in millimolar): NaCl, 115; KCl, 3.1; $MgSO_4$, 2.5; glucose, 6; Na-succinate, 1; Na-malate, 1; Na-lactate, 1; Na-pyruvate, 1; $CaCl_2$, 2; and $NaHCO_3$, 25; with 0.05% phenol red and was equilibrated with 5% CO_2/95% O_2 to a pH of 7.4. Picrotoxin (50 μM) and strychnine (10 μM) were included in the bath during voltage but not current-clamp recordings. The patch pipette solution for both the cone and bipolar cell during cell-pair recordings contained (in millimolar): KCl, 120; Cs-EGTA, 10; $MgSO_4$, 5; HEPES, 10; ATP, 5; and GTP, 0.5 (pH 7.3) with KOH. For experiments that measured bipolar cell light responses, the first two components of the solution were changed: K-methylsulfate, 112; KCl, 8; and K-EGTA, 10. For cone capacitance measurements, the first component was changed: CsCl, 112; KCl, 8; and pH was adjusted with CsOH. Intracellular solutions contained either Alexa Fluor 488 (0.2 mM; Invitrogen) or 0.5% Neurobiotin (Vector Laboratories) for subsequent visualization of cones and bipolar cells in fixed slices using immunohistochemistry. Solutions were corrected to 285 ± 5 mOsm. Experiments were performed at 32–33°C which is 4–5°C lower than non-hibernating body temperature. Although glutamate transporters have a temperature coefficient (Q10) of ~3, this temperature difference should not affect cone cleft glutamate concentrations during a brief EPSC insofar as the putative cone transporter, EAAT5, has a relatively slow turnover rate (~1 s; Gameiro et al., 2011), and the processes of EAAT1-expressing Müller glial cells surround cones but do not enter the cleft. Chemicals were obtained from Sigma-Aldrich unless indicated otherwise. Values are mean ± SEM. Retinas were stimulated with a 574-nm LED attached to a microscope video port. LED intensity was controlled by pulse-width modulation and calibrated with a photodiode detector (International Light) positioned beneath the microscope objective. Intensity was converted to equivalent photons at the peak absorbance (λ_{max} = 520 nm) for the ground squirrel green cone pigment (Kraft, 1988).

Membrane Capacitance Measurements

Membrane capacitance was measured with a HEKA EPC-10 using the "sine+dc" Lockin routine in PATCHMASTER software. A 1-kHz sinusoidal voltage command (mean = −70 ± 10 mV) was applied during two 0.5-s periods that were separated by an interval consisting, in sequence, of a 20-ms pause, a 1-ms depolarization, and a 20-ms pause. Traces were sampled at 20 kHz and low-pass filtered at 2.8 kHz. Whole-cell pipette tips were coated with Sylgard, and access resistance was 20–25 MΩ. TBOA (400 μM; Tocris Bioscience) and CsCl (5 mM) were added to the external solution to block the

cone glutamate transporter and the hyperpolarization-activated cation current (I_h), respectively. For paired recordings, bipolar cell membrane potential was maintained at −70 mV with an Axopatch 200B.

Synapse Model

The model synapse was constructed using Blender 2.49 (http://www.blender.org) and imported into MCell 3 for the Monte Carlo simulation (Kerr et al., 2008; Stiles and Bartol, 2001). The model structure (Figures 7A and 7B; Figure S1) was based on published EM reconstructions of the cone terminal. For details about both the dimensions of the synapse model and the number and location of glutamate receptors, see the Supplemental Experimental Procedures. For the Monte Carlo simulation, time steps were 1 μs and data points were averages from 50 independent runs. Vesicles contained 4,000 glutamate molecules unless stated otherwise (see Supplemental Experimental Procedures for justification). The glutamate diffusion constant was 0.33×10^{-5} cm^2-s^{-1} (Nielsen et al., 2004) unless stated otherwise. The AMPA receptor model was adapted from Häusser and Roth (1997). To address receptor saturation, which depends largely upon glutamate affinity and less upon the decay phase of the EPSC, we first modified the rate constants to decrease the EC_{50} for glutamate from 440 to 340 μM (Figure S2A). Without further adjustment, both the rise and decay of the simulated miniature EPSC (mEPSC) were slower than the rise and decay of the cb2 cell mEPSC. To match the rising phase, the scheme was further modified (Figure S2B).

SUPPLEMENTAL INFORMATION

Supplemental Information includes Supplemental Experimental Procedures, five supplemental figures, and two tables can be found with this article online at http://dx.doi.org/10.1016/j.neuron.2016.05.019.

AUTHOR CONTRIBUTIONS

Experiments and data analysis, C.P.G., A.C.L., and S.H.D.; modeling, C.P.R.; writing, C.P.G., C.P.R., and S.H.D.

ACKNOWLEDGMENTS

This work was supported by NIH grant EY012141 (S.H.D.) and Research to Prevent Blindness.

Received: April 16, 2015
Revised: February 26, 2016
Accepted: May 5, 2016
Published: June 9, 2016

REFERENCES

Babai, N., Bartoletti, T.M., and Thoreson, W.B. (2010). Calcium regulates vesicle replenishment at the cone ribbon synapse. J. Neurosci. *30*, 15866–15877.

Baden, T., Berens, P., Bethge, M., and Euler, T. (2013). Spikes in mammalian bipolar cells support temporal layering of the inner retina. Curr. Biol. *23*, 48–52.

Baden, T., Berens, P., Franke, K., Román Rosón, M., Bethge, M., and Euler, T. (2016). The functional diversity of retinal ganglion cells in the mouse. Nature *529*, 345–350.

Bartoletti, T.M., Babai, N., and Thoreson, W.B. (2010). Vesicle pool size at the salamander cone ribbon synapse. J. Neurophysiol. *103*, 419–423.

Cao, L.H., Luo, D.G., and Yau, K.W. (2014). Light responses of primate and other mammalian cones. Proc. Natl. Acad. Sci. USA *111*, 2752–2757.

Chanda, S., and Xu-Friedman, M.A. (2010). A low-affinity antagonist reveals saturation and desensitization in mature synapses in the auditory brain stem. J. Neurophysiol. *103*, 1915–1926.

Chen, S., and Diamond, J.S. (2002). Synaptically released glutamate activates extrasynaptic NMDA receptors on cells in the ganglion cell layer of rat retina. J. Neurosci. *22*, 2165–2173.

Choi, S.Y., Borghuis, B.G., Rea, R., Levitan, E.S., Sterling, P., and Kramer, R.H. (2005). Encoding light intensity by the cone photoreceptor synapse. Neuron *48*, 555–562.

Chun, M.H., Grünert, U., Martin, P.R., and Wässle, H. (1996). The synaptic complex of cones in the fovea and in the periphery of the macaque monkey retina. Vision Res. *36*, 3383–3395.

Cleland, B.G., Dubin, M.W., and Levick, W.R. (1971). Sustained and transient neurones in the cat's retina and lateral geniculate nucleus. J. Physiol. *217*, 473–496.

Derrington, A.M., and Lennie, P. (1984). Spatial and temporal contrast sensitivities of neurones in lateral geniculate nucleus of macaque. J. Physiol. *357*, 219–240.

DeVries, S.H. (2000). Bipolar cells use kainate and AMPA receptors to filter visual information into separate channels. Neuron *28*, 847–856.

DeVries, S.H. (2001). Exocytosed protons feedback to suppress the Ca^{2+} current in mammalian cone photoreceptors. Neuron *32*, 1107–1117.

DeVries, S.H., and Schwartz, E.A. (1999). Kainate receptors mediate synaptic transmission between cones and 'Off' bipolar cells in a mammalian retina. Nature *397*, 157–160.

DeVries, S.H., Li, W., and Saszik, S. (2006). Parallel processing in two transmitter microenvironments at the cone photoreceptor synapse. Neuron *50*, 735–748.

Diamond, J.S., and Jahr, C.E. (1997). Transporters buffer synaptically released glutamate on a submillisecond time scale. J. Neurosci. *17*, 4672–4687.

Dong, C.J., and Werblin, F.S. (1998). Temporal contrast enhancement via GABAC feedback at bipolar terminals in the tiger salamander retina. J. Neurophysiol. *79*, 2171–2180.

Dowling, J.E., and Boycott, B.B. (1966). Organization of the primate retina: electron microscopy. Proc. R. Soc. Lond. B Biol. Sci. *166*, 80–111.

Dunn, F.A., and Rieke, F. (2008). Single-photon absorptions evoke synaptic depression in the retina to extend the operational range of rod vision. Neuron *57*, 894–904.

Eggers, E.D., and Lukasiewicz, P.D. (2011). Multiple pathways of inhibition shape bipolar cell responses in the retina. Vis. Neurosci. *28*, 95–108.

Euler, T., and Masland, R.H. (2000). Light-evoked responses of bipolar cells in a mammalian retina. J. Neurophysiol. *83*, 1817–1829.

Foster, K.A., Kreitzer, A.C., and Regehr, W.G. (2002). Interaction of postsynaptic receptor saturation with presynaptic mechanisms produces a reliable synapse. Neuron *36*, 1115–1126.

Gameiro, A., Braams, S., Rauen, T., and Grewer, C. (2011). The discovery of slowness: low-capacity transport and slow anion channel gating by the glutamate transporter EAAT5. Biophys. J. *100*, 2623–2632.

Grabner, C.P., and Zenisek, D. (2013). Amperometric resolution of a prespike stammer and evoked phases of fast release from retinal bipolar cells. J. Neurosci. *33*, 8144–8158.

Harrison, J., and Jahr, C.E. (2003). Receptor occupancy limits synaptic depression at climbing fiber synapses. J. Neurosci. *23*, 377–383.

Häusser, M., and Roth, A. (1997). Dendritic and somatic glutamate receptor channels in rat cerebellar Purkinje cells. J. Physiol. *501*, 77–95.

Helmstaedter, M., Briggman, K.L., Turaga, S.C., Jain, V., Seung, H.S., and Denk, W. (2013). Connectomic reconstruction of the inner plexiform layer in the mouse retina. Nature *500*, 168–174.

Hopkins, J.M., and Boycott, B.B. (1997). The cone synapses of cone bipolar cells of primate retina. J. Neurocytol. *26*, 313–325.

Ichinose, T., and Hellmer, C.B. (2015). Differential signalling and glutamate receptor compositions in the OFF bipolar cell types in the mouse retina. J. Physiol. *594*, 883–894.

Ichinose, T., Shields, C.R., and Lukasiewicz, P.D. (2005). Sodium channels in transient retinal bipolar cells enhance visual responses in ganglion cells. J. Neurosci. *25*, 1856–1865.

Innocenti, B., and Heidelberger, R. (2008). Mechanisms contributing to tonic release at the cone photoreceptor ribbon synapse. J. Neurophysiol. *99*, 25–36.

Jackman, S.L., Choi, S.Y., Thoreson, W.B., Rabl, K., Bartoletti, T.M., and Kramer, R.H. (2009). Role of the synaptic ribbon in transmitting the cone light response. Nat. Neurosci. *12*, 303–310.

Jacobs, G.H., Blakeslee, B., Mccourt, M.E., and Tootell, R.B.H. (1980). Visual sensitivity of ground-squirrels to spatial and temporal luminance variations. J. Comp. Physiol. *136*, 291–299.

Kastner, D.B., and Baccus, S.A. (2014). Insights from the retina into the diverse and general computations of adaptation, detection, and prediction. Curr. Opin. Neurobiol. *25*, 63–69.

Kerr, R.A., Bartol, T.M., Kaminsky, B., Dittrich, M., Chang, J.C., Baden, S.B., Sejnowski, T.J., and Stiles, J.R. (2008). Fast Monte Carlo simulation methods for biological reaction-diffusion systems in solution and on surfaces. SIAM J. Sci. Comput. *30*, 3126–3149.

Kim, J.S., Greene, M.J., Zlateski, A., Lee, K., Richardson, M., Turaga, S.C., Purcaro, M., Balkam, M., Robinson, A., Behabadi, B.F., et al.; EyeWirers (2014). Space-time wiring specificity supports direction selectivity in the retina. Nature *509*, 331–336.

Koike-Tani, M., Saitoh, N., and Takahashi, T. (2005). Mechanisms underlying developmental speeding in AMPA-EPSC decay time at the calyx of Held. J. Neurosci. *25*, 199–207.

Kraft, T.W. (1988). Photocurrents of cone photoreceptors of the golden-mantled ground squirrel. J. Physiol. *404*, 199–213.

Lagnado, L. (1998). Retinal processing: amacrine cells keep it short and sweet. Curr. Biol. *8*, R598–R600.

Li, W., and DeVries, S.H. (2006). Bipolar cell pathways for color and luminance vision in a dichromatic mammalian retina. Nat Neurosci. *9*, 669–675.

Light, A.C., Zhu, Y., Shi, J., Saszik, S., Lindstrom, S., Davidson, L., Li, X., Chiodo, V.A., Hauswirth, W.W., Li, W., and DeVries, S.H. (2012). Organizational motifs for ground squirrel cone bipolar cells. J. Comp. Neurol. *520*, 2864–2887.

Lindstrom, S.H., Ryan, D.G., Shi, J., and DeVries, S.H. (2014). Kainate receptor subunit diversity underlying response diversity in retinal off bipolar cells. J. Physiol. *592*, 1457–1477.

Ma, Y.P., Cui, J., and Pan, Z.H. (2005). Heterogeneous expression of voltage-dependent Na^+ and K^+ channels in mammalian retinal bipolar cells. Vis. Neurosci. *22*, 119–133.

Mennerick, S., and Matthews, G. (1996). Ultrafast exocytosis elicited by calcium current in synaptic terminals of retinal bipolar neurons. Neuron *17*, 1241–1249.

Neef, A., Khimich, D., Pirih, P., Riedel, D., Wolf, F., and Moser, T. (2007). Probing the mechanism of exocytosis at the hair cell ribbon synapse. J Neurosci. *27*, 12933–12944.

Neher, E., and Sakaba, T. (2001). Combining deconvolution and noise analysis for the estimation of transmitter release rates at the calyx of held. J. Neurosci. *21*, 444–461.

Nielsen, T.A., DiGregorio, D.A., and Silver, R.A. (2004). Modulation of glutamate mobility reveals the mechanism underlying slow-rising AMPAR EPSCs and the diffusion coefficient in the synaptic cleft. Neuron *42*, 757–771.

Oesch, N.W., and Diamond, J.S. (2011). Ribbon synapses compute temporal contrast and encode luminance in retinal rod bipolar cells. Nat. Neurosci. *14*, 1555–1561.

Palmer, M.J., Hull, C., Vigh, J., and von Gersdorff, H. (2003). Synaptic cleft acidification and modulation of short-term depression by exocytosed protons in retinal bipolar cells. J Neurosci. *23*, 11332–11341.

Pang, J.J., Gao, F., Paul, D.L., and Wu, S.M. (2012). Rod, M-cone and M/S-cone inputs to hyperpolarizing bipolar cells in the mouse retina. J. Physiol. *590*, 845–854.

Patneau, D.K., Vyklicky, L., Jr., and Mayer, M.L. (1993). Hippocampal neurons exhibit cyclothiazide-sensitive rapidly desensitizing responses to kainate. J. Neurosci. *13*, 3496–3509.

Puthussery, T., Venkataramani, S., Gayet-Primo, J., Smith, R.G., and Taylor, W.R. (2013). NaV1.1 channels in axon initial segments of bipolar cells augment input to magnocellular visual pathways in the primate retina. J. Neurosci. *33*, 16045–16059.

Rabl, K., Cadetti, L., and Thoreson, W.B. (2005). Kinetics of exocytosis is faster in cones than in rods. J. Neurosci. *25*, 4633–4640.

Rabl, K., Cadetti, L., and Thoreson, W.B. (2006). Paired-pulse depression at photoreceptor synapses. J. Neurosci. *26*, 2555–2563.

Sagdullaev, B.T., McCall, M.A., and Lukasiewicz, P.D. (2006). Presynaptic inhibition modulates spillover, creating distinct dynamic response ranges of sensory output. Neuron *50*, 923–935.

Sampath, A.P., and Rieke, F. (2004). Selective transmission of single photon responses by saturation at the rod-to-rod bipolar synapse. Neuron *41*, 431–443.

Saszik, S., and DeVries, S.H. (2012). A mammalian retinal bipolar cell uses both graded changes in membrane voltage and all-or-nothing Na^+ spikes to encode light. J. Neurosci. *32*, 297–307.

Sheng, Z., Choi, S.Y., Dharia, A., Li, J., Sterling, P., and Kramer, R.H. (2007). Synaptic Ca^{2+} in darkness is lower in rods than cones, causing slower tonic release of vesicles. J. Neurosci. *27*, 5033–5042.

Singer, J.H., and Diamond, J.S. (2003). Sustained Ca^{2+} entry elicits transient postsynaptic currents at a retinal ribbon synapse. J. Neurosci. *23*, 10923–10933.

Singer, J.H., and Diamond, J.S. (2006). Vesicle depletion and synaptic depression at a mammalian ribbon synapse. J. Neurophysiol. *95*, 3191–3198.

Smith, V.C., Pokorny, J., Lee, B.B., and Dacey, D.M. (2001). Primate horizontal cell dynamics: an analysis of sensitivity regulation in the outer retina. J. Neurophysiol. *85*, 545–558.

Sterling, P., and Matthews, G. (2005). Structure and function of ribbon synapses. Trends Neurosci. *28*, 20–29.

Stiles, J.R., and Bartol, T.M. (2001). Monte Carlo methods for simulating realistic synaptic microphysiology using MCell. In Computational Neuroscience: Realistic Modeling for Experimentalists, E. De Schutter, ed. (CRC Press), pp. 87–127.

Sun, J.Y., and Wu, L.G. (2001). Fast kinetics of exocytosis revealed by simultaneous measurements of presynaptic capacitance and postsynaptic currents at a central synapse. Neuron *30*, 171–182.

Tansley, K. (1965). Vision in Vertebrates (Chapman and Hall).

Tsukamoto, Y., and Omi, N. (2015). OFF bipolar cells in macaque retina: type-specific connectivity in the outer and inner synaptic layers. Front. Neuroanat. *9*, 122.

von Gersdorff, H., Sakaba, T., Berglund, K., and Tachibana, M. (1998). Submillisecond kinetics of glutamate release from a sensory synapse. Neuron *21*, 1177–1188.

Wadiche, J.I., and Jahr, C.E. (2001). Multivesicular release at climbing fiber-Purkinje cell synapses. Neuron *32*, 301–313.

Neuron, Volume *91*

Supplemental Information

Mechanism of High-Frequency Signaling at a Depressing Ribbon Synapse

Chad P. Grabner, Charles P. Ratliff, Adam C. Light, and Steven H. DeVries

Supplemental Data

Figure S1

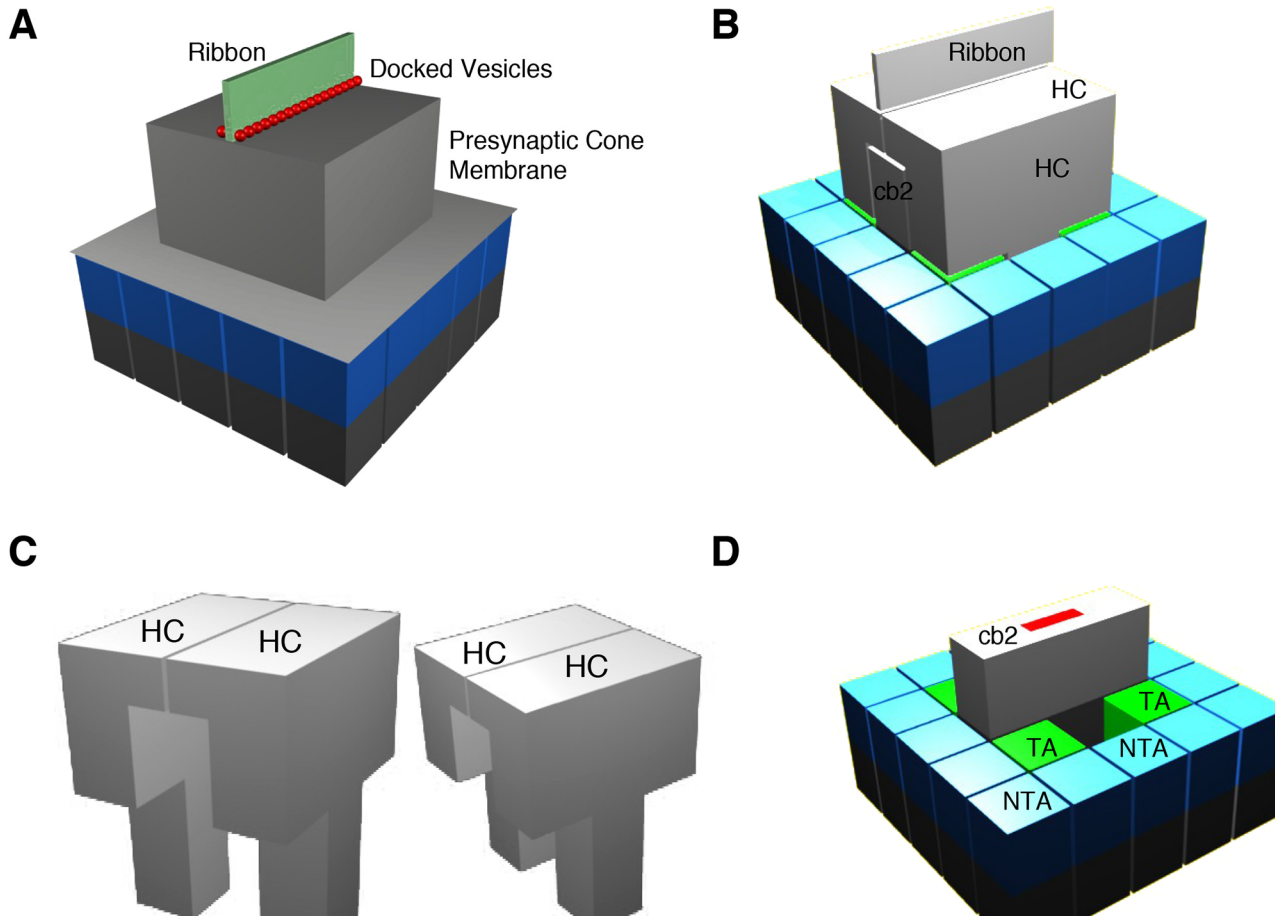

Figure S1, related to Figure 7: Model of the cone synapse. **A.** Ribbon (green) with docked vesicles (red) sits atop a single invagination of the presynaptic cone membrane (gray box). The basal synaptic surface is composed of bipolar cell dendritic contacts (dark gray and blue). In our simulations, the presynaptic membrane was first extended horizontally, then downward, and then horizontally again to cover the basal contacts as a sheet. **B.** Similar view to Figure 7A with the presynaptic cone terminal membrane and vesicles removed. The ribbon is maintained as a landmark. Glutamate released at the ribbon may diffuse both centrally and laterally between and around the horizontal cell (HC) processes to reach the basal postsynaptic surface. **C.** HC processes, shown from two different angles, occupy the bulk of the volume of the invagination. The AMPA receptors on HCs were not included in the model. **D.** Postsynaptic bipolar cells (right) with ribbon and HC processes removed. A single, invaginating bipolar cell contact (light grey) expressing AMPA receptors (red) was used instead of several separate invaginating contacts, some from On bipolar cells, so as to study differences in receptor placement. The basal region shows two types of bipolar cell processes. The green contacts below the removed HC processes (triad associated, TA) are closer to the invagination or triad than the blue bipolar cell contacts (non-TA, NTA), and were separately analyzed. For the present work, we note that neither type of basal process exhibited saturation.

Figure S2

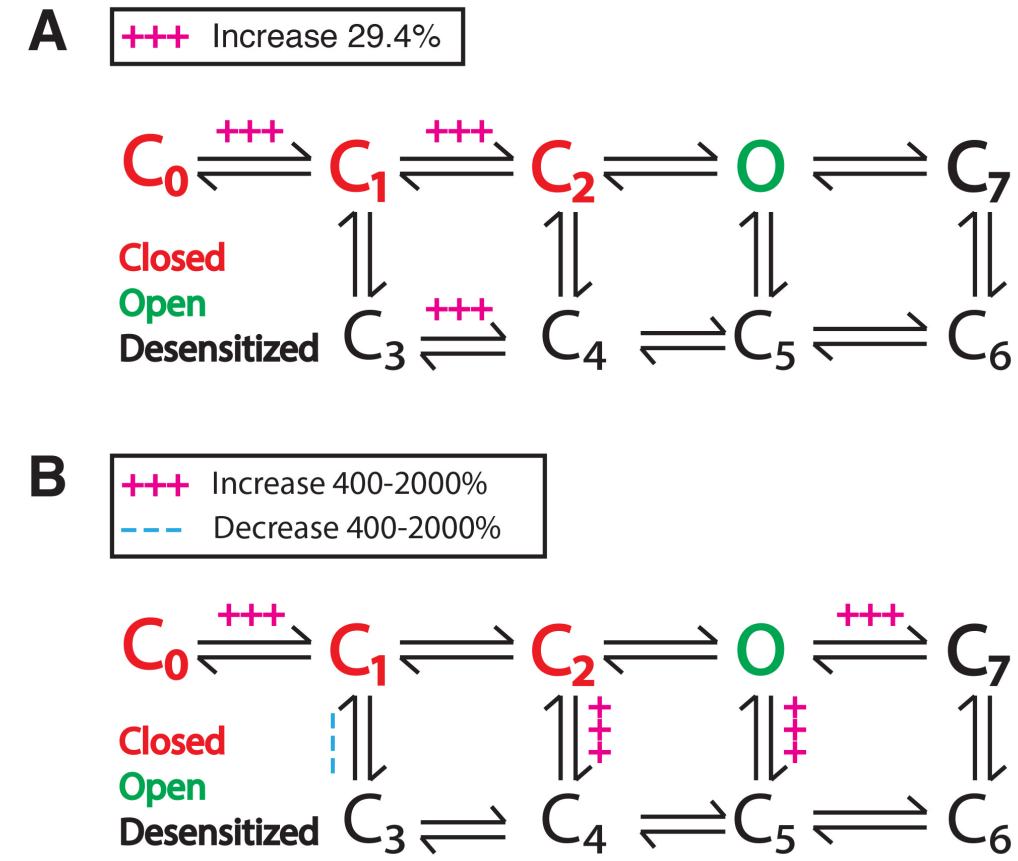

Figure S2, related to Figure 7: Since our goal was to address receptor saturation, which depends largely upon glutamate affinity and much less upon the decay phase of the EPSC, we initially modified the rate constants of the Häusser & Roth (1997) model to increase the affinity for glutamate from 440 to 340 μM. **A.** To increase affinity, the rate constants C_0-->C_1, C_1-->C_2 and C_3-->C_4 which involve glutamate binding were all increased by 29.4%. We increased the 'on' instead of decreasing the 'off' rates to better match the faster time course of the experimental mEPSC. Changing C_0-->C_1 alone, even by up to 1000-fold, had only a minor effect on response shape. **B.** Without further adjustment, the decay phase of the simulated mEPSC was still slower than the decay phase of the cb2 cell mEPSC (see Figure S3). The scheme was further modified to increase the rate of exit from the open state or the decay phase of the mEPSC, while preserving microscopic reversibility (DiGregorio et al., 2007).

Figure S3

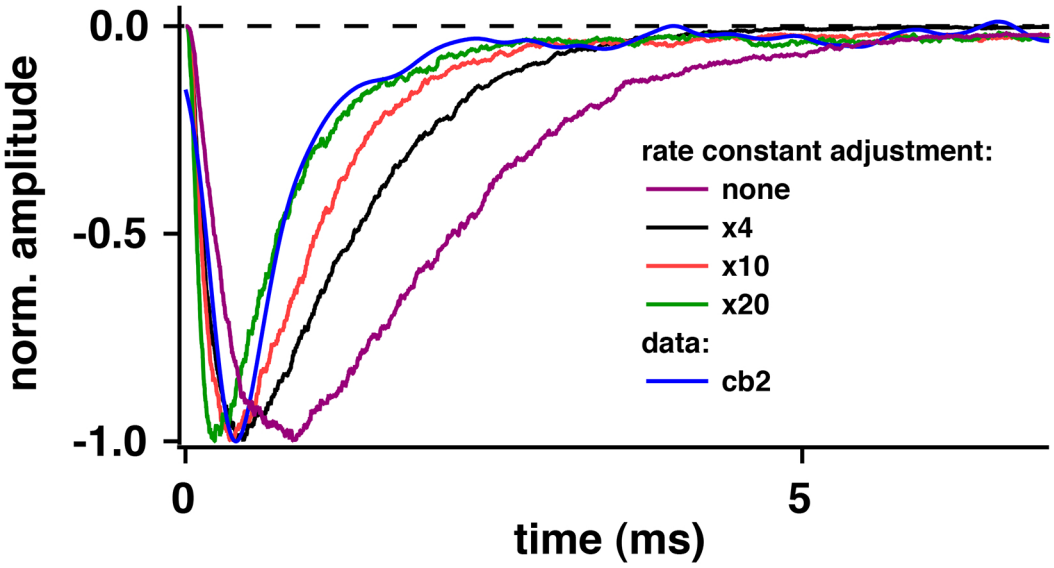

Figure S3, related to Figure 7: Speeding up the mEPSC time course. After making the affinity adjustment, we sought to match the response rise. A 10-fold increase in rate constant was selected as providing the best match between experimental and simulated events. The rate constants in Figure S2B were modified accordingly. The effects on saturation of making this second set of adjustments were minimal: EC_{50} was 3.4 versus 3.3 vesicles before and after the receptor modifications (data not shown; simulated with each vesicle containing 3000 glutamate molecules).

Figure S4

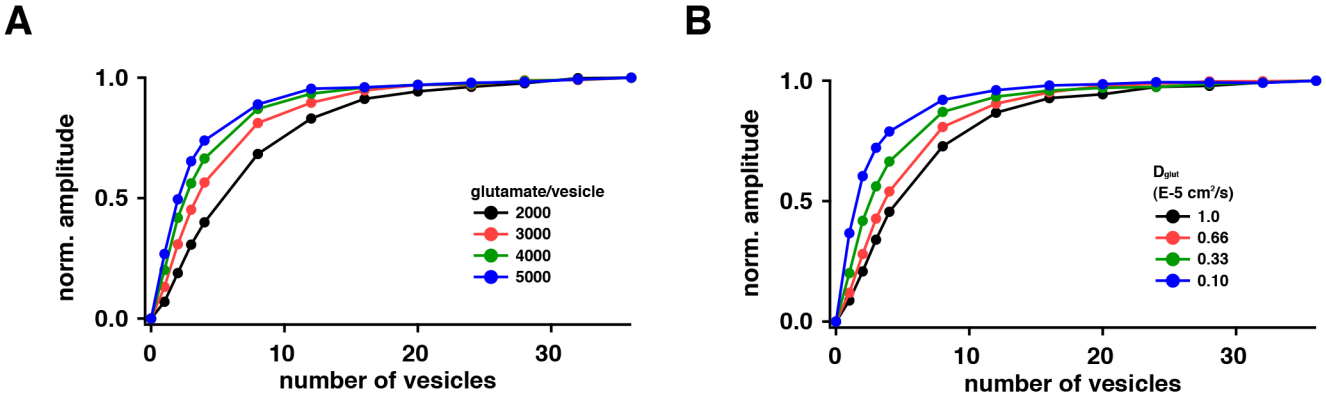

Figure S4, related to Figure 7: Control simulations of receptor saturation at the cone to cb2 cell synapse. **A.** Normalized EPSC amplitude versus number of vesicles released for different values of vesicular glutamate content. We varied the vesicular glutamate content from 2000 to 5000 per vesicle to ensure that receptor saturation was robust to the experimental uncertainty in estimating this quantity. **B.** Normalized EPSC amplitude versus number of vesicles released for different values of the glutamate diffusion constant.

Figure S5

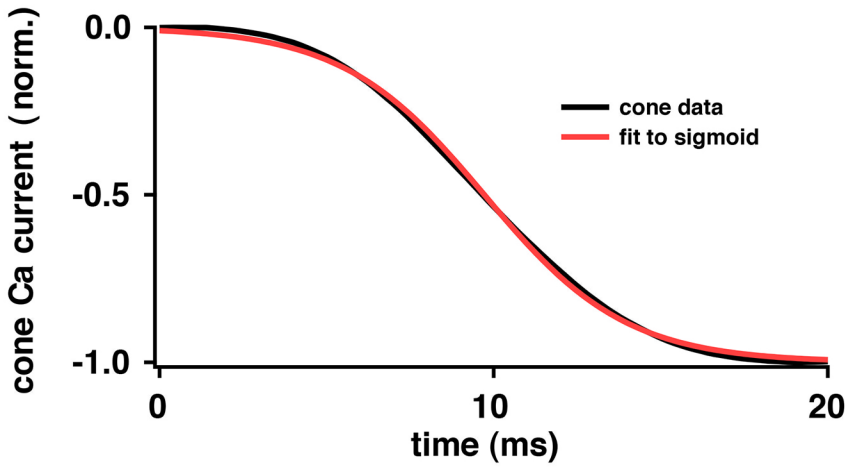

Figure S5, related to Figure 7: Time course of Ca^{2+} current activation at light-off with data fit to a sigmoid. The time course of the cone membrane voltage response at light-off was obtained from the traces in Figure 2 (*inset*). Membrane voltage was converted to Ca^{2+} current using the cone Ca^{2+} I-V relation (DeVries and Schwartz, 1999). The cone Ca^{2+} current versus time plot was fitted with a sigmoid. The sigmoid was taken as the cumulative probability distribution function for vesicle release times, and the vesicle release times used for each independent simulation were drawn randomly from this distribution.

Condition	Pulse duration (ms)	Recovery t (ms)	±SEM	n	p*
whole cell					
BAPTA, 10 mM	15	154.9	30	4	-
EGTA, 10 mM	1-15	133.5	23.3	8	-
loose seal	1	105.4	13.1	12	-
	5-15	125.1	22.8	6	-

*Wilconxon rank-sum test

Table S1, related to Figure 2: Recording conditions that can change the intracellular Ca^{2+} concentration or buffering do not affect paired pulse recovery. Paired pulse recovery at cone to cb2 cell synapses was statistically indistinguishable with respect to cone recording mode, whole cell or loose seal, duration of the cone step (1 – 15 ms), or intracellular Ca^{2+} buffer type, BAPTA or EGTA, both 10 mM. (-) indicates that none of the conditions produce statistically distinct results.

Condition	Control	CTZ (50-60 μM)	n	p*
Recovery tau (ms)	149.7±26.1	135.5±12.9	5	0.43
Peak amplitude (pA)	-311.3±64.4	-319.9±69.5	7	0.52

*Paired t test

Table S2, related to Figure 2: Effects of CTZ on paired-pulse recovery time course and EPSC amplitude. Recovery and control values were statistically indistinguishable.

Supplemental Experimental Procedures

Synapse model

The model synapse was based on published EM reconstructions of the cone terminal (Dowling and Boycott, 1966; Herr et al., 2011; Schein et al., 2011; Sterling and Matthews, 2005). The model featured a synaptic ribbon, a cone membrane that formed the presynaptic side of the cleft, two invaginating horizontal cell processes, and three types of bipolar cell processes: central (invaginating), triad-associated (TA, semi-invaginating), and non-triad-associated (NTA, basal). Vesicles were spaced 40 nm apart on both sides of the ribbon, invagination depth was 500 nm, bipolar cell contacts at the cone base were spaced 250 nm apart, and cleft width was 16 nm**.** Two horizontal cell processes abut at the base of the ribbon to form a sheet-like cleft through which glutamate can diffuse from ribbon to postsynaptic cb2 bipolar cell receptors. The receptors on the cb2 cells occupy a central patch that has 1/9 of the area of the entire surface (0.019 μm^2). Changing the size of this patch had only a small effect on the approach to saturation. We used the MCell default density for the AMPA receptors, 10,000-μm^{-2} (Stiles et al., 1996). For comparison, the maximal packing density of tetrameric GluA2-containing AMPA receptors is estimated to be 7400-μm^{-2} (Sobolevsky et al., 2009). We assumed that glutamate was instantaneously released upon vesicle fusion in line with empirical results from amperometric measurements at ribbon synapses (Grabner and Zenisek, 2013). Glutamate was absorbed upon diffusing 500 nm below the basal contact surface.

Estimating the number of vesicles released per ribbon to produce a threshold response in a cb2 cell

We calculated the number of vesicles released per ribbon to produce a threshold response in a cb2 bipolar cell as follows: The dynamic range for cb2 cell light response transients at low frequencies is on average 30.7 mV (Figure 1A). Using the relationship between cone capacitance change and cb2 EPSC amplitude figure Figure 5D, we infer that the midpoint of this range, 15.35 mV, corresponds to 2.3 vesicles released per ribbon ($\Delta C_{m(1/2)}$ = 2.3 fF, 0.05 fF/vesicle, and 20 ribbons per cone). We assign a threshold for transmitter release of 2 – 3 mV at the bipolar cell terminal, which, by linear extrapolation, corresponds to the release of roughly 0.3 – 0.45 vesicles per ribbon in the cones presynaptic to the recorded cb2 cell.

Estimating the number of glutamate molecules in a cone vesicle

The precise number of glutamate molecules in a cone vesicle is difficult to determine. We approached the problem by estimating the number of channels at a cb2 cell cone contact that are opened during the peak real mEPSC response and compared that to the number of channels that are opened by different vesicular glutamate concentrations in simulations. The maximal cb2 EPSC amplitude in our dataset was 378.5 ± 257.8 pA (n = 60 cells). The mean number of cb2 contacts per cone was 8.28 ± 4.76 (n = 4 cb2 cells and 41 contacted cones), so that the maximal EPSC amplitude per contact was 45.7 pA. Assuming a single-channel conductance of 12 pS (Ashby et al., 2008) and a reversal potential for bipolar cell cation channels of 0 mV, while noting that bipolar cells in these experiments were voltage-clamped at – 70 mV, we calculate that the single channel current is 70 mV x 12 pS = 0.84 pA. Thus 45.7/0.84 = 54.4 channels open on a single contact during a saturating glutamate pulse. Since we maximum open probability for the channel is ~70% (DeVries et al., 2006), we calculate that ~78 channels are expressed per dendritic tip. The mean cb2 mEPSC amplitude is 9.9 pA (DeVries et al., 2006), suggesting that the mEPSC opens almost a fourth of the maximum possible number of channels. In our simulations, this amplitude corresponds to 4000 glutamate molecules per vesicle, which is a reasonable value based on the range of values encountered in the literature (Barbour and Hausser, 1997; Budisantoso et al., 2013; Clements, 1996; DiGregorio et al., 2007; Jonas et al., 1993; Nielsen et al., 2004; Rao-Mirotznik et al., 1998; Riveros et al., 1986; Savtchenko et al., 2013). This is the concentration of glutamate that we chose. Other efforts, based on measurements of vesicular glutamate concentration and vesicle diameter, have led to two-fold lower estimates of glutamate concentration at the rod ribbon (Rao-Mirotznik et al., 1998). Matching our data to these estimates would require revision of our synapse geometry, our kinetic model, or our estimate for AMPAR single channel conductance.

Supplemental References

Ashby, M.C., Daw, M.I., and Isaac, J.T.R. (2008). AMPA Receptors. In The Glutamate Receptors, R.W. Gereau, and G.T. Swanson, eds. (Humana Press), pp. 1-44.

Barbour, B., and Hausser, M. (1997). Intersynaptic diffusion of neurotransmitter. Trends Neurosci 20, 377-384.

Budisantoso, T., Harada, H., Kamasawa, N., Fukazawa, Y., Shigemoto, R., and Matsui, K. (2013). Evaluation of glutamate concentration transient in the synaptic cleft of the rat calyx of Held. J Physiol 591, 219-239.

Clements, J.D. (1996). Transmitter timecourse in the synaptic cleft: its role in central synaptic function. Trends Neurosci 19, 163-171.

DiGregorio, D.A., Rothman, J.S., Nielsen, T.A., and Silver, R.A. (2007). Desensitization properties of AMPA receptors at the cerebellar mossy fiber granule cell synapse. J Neurosci 27, 8344-8357.

Herr, S., Ngo, I.T., Huang, T.M., Klug, K., Sterling, P., and Schein, S. (2011). Cone synapses in macaque fovea: II. Dendrites of OFF midget bipolar cells exhibit Inner Densities similar to their Outer synaptic Densities in basal contacts with cone terminals. Vis Neurosci 28, 17-28.

Jonas, P., Major, G., and Sakmann, B. (1993). Quantal components of unitary EPSCs at the mossy fibre synapse on CA3 pyramidal cells of rat hippocampus. J Physiol 472, 615-663.

Rao-Mirotznik, R., Buchsbaum, G., and Sterling, P. (1998). Transmitter concentration at a three-dimensional synapse. J Neurophysiol 80, 3163-3172.

Riveros, N., Fiedler, J., Lagos, N., Munoz, C., and Orrego, F. (1986). Glutamate in rat brain cortex synaptic vesicles: influence of the vesicle isolation procedure. Brain Res 386, 405-408.

Savtchenko, L.P., Sylantyev, S., and Rusakov, D.A. (2013). Central synapses release a resource-efficient amount of glutamate. Nat Neurosci 16, 10-12.

Schein, S., Ngo, I.T., Huang, T.M., Klug, K., Sterling, P., and Herr, S. (2011). Cone synapses in macaque fovea: I. Two types of non-S cones are distinguished by numbers of contacts with OFF midget bipolar cells. Vis Neurosci 28, 3-16.

Sobolevsky, A.I., Rosconi, M.P., and Gouaux, E. (2009). X-ray structure, symmetry and mechanism of an AMPA-subtype glutamate receptor. Nature 462, 745-756.

Stiles, J.R., Van Helden, D., Bartol, T.M., Jr., Salpeter, E.E., and Salpeter, M.M. (1996). Miniature endplate current rise times less than 100 microseconds from improved dual recordings can be modeled with passive acetylcholine diffusion from a synaptic vesicle. Proc Natl Acad Sci U S A 93, 5747-5752.